Geological Quarterly, 2023, 67: 14
DOI: http://dx.doi.org/10.7306/gq.1684

Provenance and tectonic setting of the Middle Eocene lower Akhoreh Formation, Nain area, Central Iran, assessed using petrography and geochemistry

Mohammad Ali SALEHI[1, *], Mohammad MALLAH[1] and Mahdi JAFARZADEH[2]

[1] University of Isfahan, Faculty of Sciences, Department of Geology, ISFAHAN 81744, Iran; ORCID: 0000-0001-8670-5973 [M.A.S.], 0009-0003-3727-526X [M.M.]

[2] Shahrood University of Technology, Faculty of Earth Sciences, Shahrood, Iran; ORCID: 0000-0002-0542-9215

Salehi, M.A., Mallah, M., Jafarzadeh, M., 2023. Provenance and tectonic setting of the Middle Eocene lower Akhoreh Formation, Nain area, central Iran, assessed using petrography and geochemistry. Geological Quarterly, 67: 14, doi: 10.7306/gq.1684

The Middle Eocene Akhoreh Formation is superbly exposed in the western corner of the Central-East Iranian Microcontinent (CEIM). This formation covered the northeastern flank of the Cretaceous Nain Ophiolite Mélange (NOM) and is adjacent to the Paleogene Urmieh–Dokhtar Magmatic Arc (UDMA) formed in the southwest of the CEIM. This terrigenous succession is composed of a thin basal conglomerate followed by mostly pink to purple sandstones alternating with shales. The clast composition and clast imbrication of the conglomerates show local source areas towards the north-north-east. Modal components of lower Akhoreh Formation sandstones reveals immature lithic arkose ($Q_8F_{48}L_{44}$) and feldspathic litharenite ($Q_8F_{44}L_{48}$) sandstones that are rich in mafic and ultramafic igneous and volcanic rock fragments. Mafic to ultramafic source rocks are also indicated by geochemical data (enrichment of Mg, Cr and Ni and Cr/V) in the sandstone and shale samples analyzed. However, geochemical data suggests an intermediate igneous rock origin for the shale samples studied, most likely from the nearby continental arc. Based on petrographic data, these sandstones have characteristics of a transitional to undissected arc tectonic setting. Geochemical discrimination diagrams using major and trace elements indicate an oceanic island arc tectonic setting for the lower Akhoreh Formation sandstones and shales, probably due to a predominance of ophiolitic source rocks. Furthermore, the chemical index of alteration and modal analysis indicate a weak to moderate degree of chemical weathering with arid climatic conditions in the source area. The exhumed NOM, together with the UDMA in the southwest, were dominant sources of sediment to the lower Akhoreh Formation, that lay to the north-east in a local retroarc basin of the Central Iranian Microplate, during the Middle Eocene.

Key words: petrography, geochemistry, palaeogeography, Nain Ophiolite, Akhoreh Formation, Central Iran.

INTRODUCTION

The Central-East Iranian Microcontinent (CEIM) structurally consists of three units (the Lut, Tabas and Yazd blocks from east to west, respectively) with several surrounding ophiolitic suture zones, remnants of the Palaeo- and Neo-Tethys oceans (Shafaii Moghadam et al., 2009; Torabi et al., 2011). The study area lies in the western corner of the CEIM where an important ophiolitic sutures zone, the Nain Ophiolite Mélange (NOM), representing the largest and most complete Mesozoic mélange of a Neo-Tethys oceanic branch emplaced onto the continental basement, crops out (Fig. 1). This is overlain by remarkably thick early Cenozoic (Middle Eocene–earliest Oligocene) terrigenous "flysch-type deposits" which suggest marked extension. The NOM has been widely studied as regards its petrology, geochemistry, geochronology and radiolarian biostratigraphy (Davoudzadeh, 1969, 1972; Shafaii Moghadam et al., 2009; Torabi et al., 2011; Pirnia et al., 2013, 2020; Shirdashtzadeh et al., 2014, 2015; Shirdashtzadeh and Torabi, 2020). The Cenozoic succession, including the Middle Eocene–earliest Oligocene Akhoreh Formation, superbly exposed and overlying the eastern flank of the NOM, preserves important evidence of the palaeogeographic and geodynamic evolution of the CEIM. Provenance study of the siliciclastic deposits, via combined petrographic and geochemical analysis, can provide information to help reconstruct the tectonic setting, climate, weathering and parent-rock lithologies of the source area (e.g., Dickinson et al., 1983; Armstrong-Altrin et al., 2015; Garzanti and Resentini, 2016; Taheri et al., 2018; Critelli, 2018; Armstrong-Altrin, 2020; Armstrong-Altrin et al., 2021; Jafarzadeh et al., 2022). Beside the major element/oxide composition of the clastic rocks which reveal provenance, trace elements can be used to differentiate felsic and mafic parent rocks as well as indicate palaeoweathering conditions in the source area (e.g., Basu et al., 2016; Armstrong-Altrin, 2020).

Moreover, petrographical and mineralogical studies of sedimentary rocks derived from ophiolitic sequences can provide essential information about the evolution of suture belts

* Corresponding author: ma.salehi@sci.ui.ac.ir

Received: November 27, 2022; accepted: March 9, 2023; first published online: May 26, 2023

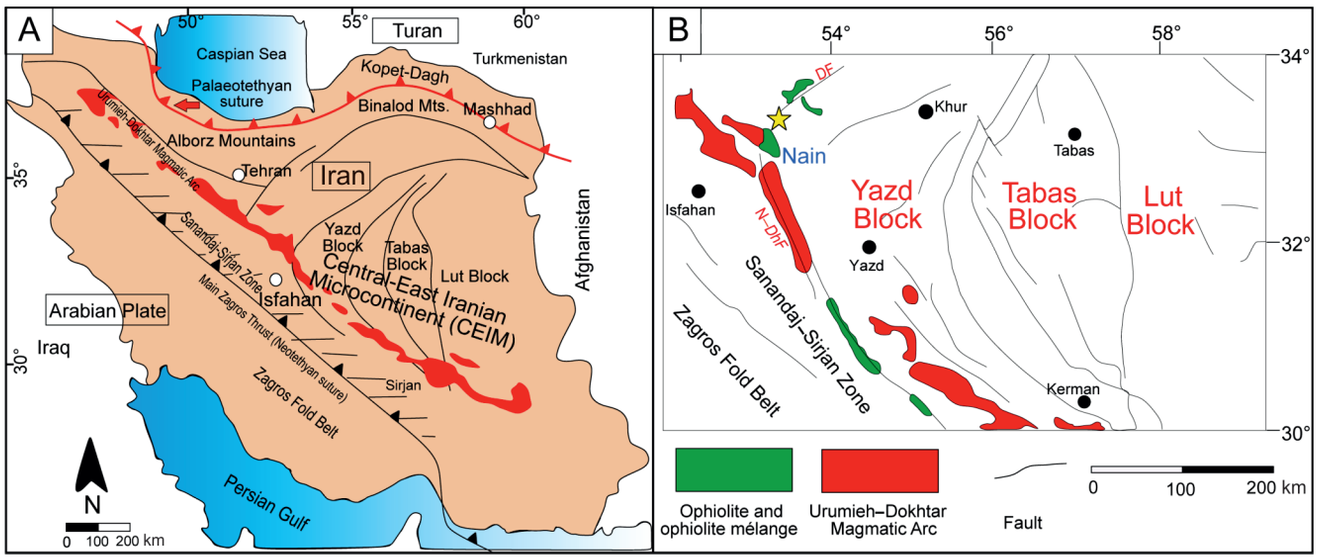

Fig. 1A – geographical and structural framework of Iran including the main structural units, sutures and geographic locations (subdivision boundaries modified from Wilmsen et al., 2009); B – CEIM and its main three structural units (the Lut, Tabas and Yazd blocks) and block bounding faults (redrawn after Ramezani and Tucker, 2003)

Asterisks indicate the approximate position of the study area; DF – Doruneh Fault; N–DhF – Nain–Dehshir Fault

(Garzanti et al., 2000, 2002; Meinhold et al., 2009; Gholami-Zadeh et al., 2017). The Akhoreh Formation, the sedimentary cover of an important obducted oceanic crustal unit, has received little attention so far (Pirnia et al., 2013). This succession has yet not been studied in detail as regards sandstone petrography or the major, trace and rare earth element geochemistry of the sandstones and shales. These sandstones and shales are very different in their characteristics, including of grain size and depositional environment, but their chemical composition can help assess provenance history in a single basin (e.g., Cullers, 2000; Salehi et al., 2014; Pourdivanbeigi Moghaddam et al., 2020).

This provenance study of the lower Akhoreh Formation, mainly recording the erosion of obducted oceanic crust, gives valuable information on the tectonic setting, weathering and parent rock lithologies of the source area, and help reconstruct the palaeogeography and geodynamic history of Central Iran during the Middle Eocene.

GEOLOGICAL SETTING

In the Late Cretaceous, there was oblique subduction of the northern part of the Neo-Tethys Ocean beneath the Iranian Plate as well as counterclockwise vertical-axis rotation within the different blocks of the CEIM; as a result, several small fringing oceanic back-arc basins, such as the Nain–Baft, Sabzevar and Sistan basins, were developed (Shafaii Moghadam et al., 2009; Kazemi et al., 2019). Arabian–Eurasian convergence led to the closure of these narrow oceanic basins during the latest Cretaceous–Paleogene. This resulted in the obduction of ophiolites along the Nain–Baft, Sabzevar and Sistan sutures onto the continental basement (Agard et al., 2011; Hassanzadeh and Wernicke, 2016). The NOM is strongly tectonized and consists of a mixture of igneous, metamorphic and sedimentary rocks. The Upper Cretaceous–Paleogene subduction-related magmatic arc termed the UDMA formed along the active margin of the southern Iran Plate, including southwest of the CEIM (Berberian and King, 1981; Chiu et al., 2013; Hassanzadeh and Wernicke, 2016). Thin neritic limestones of Middle Paleocene to Early Eocene age, containing diabase sills, rest unconformably on the pelagic limestones of the NOM. Above these, a thick (~3200 m) terrigenous succession (Akhoreh Formation) accumulated, of Middle Eocene (Lutetian)–earliest Oligocene age, consisting of an alternation of pink and green-grey marls, calcareous marls, marly shales, feldspathic sandstones and fine-grained conglomerates with a “flysch-like” appearance. These overlie the eastern part of the ophiolite mélange, while Cenozoic volcanic rocks associated with small coeval dioritic intrusions of the UDMA crop out in the west (Davoudzadeh, 1972).

Deposition of this thick terrigenous succession took place in a trough-shaped basin accompanied by normal faulting (Davoudzadeh, 1972; Davoudzadeh et al., 1997), inferred to be the result of long-lived synsedimentary subsidence with rapid deposition in a relatively shallow extensional continental back-arc basin (Davoudzadeh, 1972; Verdel et al., 2011; Barrier et al., 2018). Similarly, an extensional basin formed in the southern Alborz where the thick volcano-sedimentary Karaj Formation was deposited (Malekzadeh et al., 2020). This extension, associated with a magmatic flare-up of the UDMA, is considered to reflect southwestwards retreat of the subduction zone or slab rollback (Verdel et al., 2011; Mouthereau et al., 2012). A palaeogeographic reconstruction shows that the study area lay at a subtropical palaeolatitude of ~30° north, with an arid palaeoclimate (Barrier et al., 2018). In this reconstruction, the southwestern margin of central Iran and the CEIM was placed in an extensional continental back-arc basin with a narrow NW–SE basin stretched parallel to the Sanandaj–Sirjan Zone (Fig. 2). The obducted NOM, as well as the UDMA, were placed at the western margin of the basin (Fig. 2). Lower Oligocene– Lower Miocene continental to shallow marine deposits (Lower Red, Qom and Upper Red formations) overlie the Middle Eocene–lowermost Oligocene succession. A Late Neogene tectonic event reflecting collision between Arabia and the Iran Plate resulted in widespread upper-plate deformation and shortening (Allen et al., 2004; Tadayon et al., 2017, 2019).

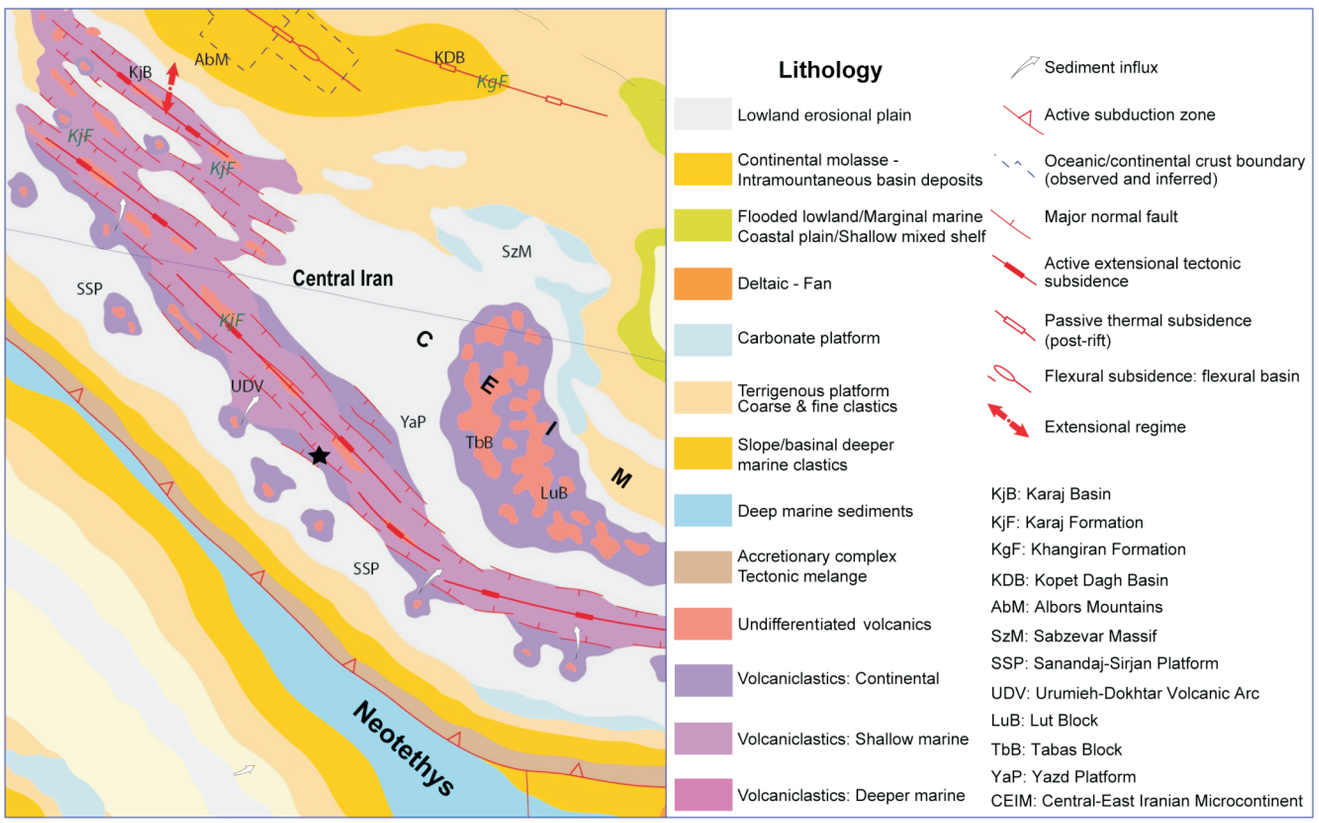

Fig. 2. A palaeogeographic and plate tectonic framework of the Middle East in the Eocene (Lutetian; modified after Barrier et al., 2018)

Note the study area during Middle Eocene with major potential source areas and sediment transport directions for the lower Akhoreh Formation in the western corner of CEIM; asterisks indicate the approximate position of the study area

MATERIAL AND METHODS

Fieldwork included measuring the stratigraphic succession selected, recording and describing the main characteristics of the rock units (i.e. lithology, sedimentary structures, geometries, pebble composition etc.; Table 1). A total of 24 samples (19 sandstone and 5 shale) as hand specimens were collected from the lowermost Akhoreh Formation. Ten palaeocurrent indicators were measured at three locations to constrain dispersal patterns. Measurement included unidirectional indica-

Table 1

Lithostratigraphic unit thickness and description of the lower Akhoreh Formation in the Shurab section to the north of Nain, Central Iran

Unit no.	Lithostratigraphic Thickness	Field description
1	45	Well-developed, mostly massive, matrix-supported conglomerate with a pinkish sandy matrix and angular to sub-angular clasts
2	103	Pebbly sandstones; pink to red, medium- to thick-bedded sandstones-siltstones and shale intercalations
3	18	Red shale and thin siltstone intercalations
4	58	Grey siltstones and red shales at base; pink and grey coarse-grained sandstones with pedogenic fabric; green shales toward the top
5	54	Pink and grey, coarse-grained sandstones with thin green and purple shale intercalations
6	48	Pink and grey trough cross-bedded, coarse-grained sandstones with purple shale intercalations
7	56	Interbedded green shales with pink horizontal laminated sandstones
8	56	Massive matrix-supported conglomerates at base; grey sandstone and pink to green shale intercalations with a fining-upwards pattern
9	36	Grey sandstone and siltstone intercalations and subordinate green shale interlayers
10	31	Thick light green shales
Total measured thickness = 505		

Table 2

Detrital grains mode of the lower Akhoreh sandstones based on Gazzi-Dickinson method at the Shurab section in the north of Nain, Central Iran

Sample	Qm non	Qm un	Qp 2-3	Qp >3	K	P	Lv	Ls	Lp	Lm	Cht	M	Porosity	Cem	Acc	Total
M1	22	4	0	5	45	66	60	10	10	5	10	35	0	22	15	309
M2	10	5	0	0	36	55	88	5	5	0	5	47	0	35	10	301
M4	12	3	0	0	45	61	75	10	0	0	10	45	0	45	15	321
M6	17	0	0	6	48	66	90	9	0	0	12	38	0	43	12	341
M7	15	2	0	4	43	66	72	12	0	6	17	32	0	50	8	327
M8	12	2	0	5	35	55	92	9	5	0	10	35	0	47	9	316
M9	21	6	0	0	37	65	70	15	0	0	15	45	0	40	11	325
M11	15	0	0	0	30	57	96	6	0	0	11	40	0	35	10	300
M13	11	1	0	0	32	67	78	10	0	3	15	39	0	44	8	308
M14	13	0	0	0	27	51	95	5	0	0	17	41	0	45	9	303
M16	8	0	0	0	38	68	71	12	0	0	12	36	0	56	12	313
M17	14	3	0	0	41	70	86	6	6	0	10	30	5	50	8	329
M18	16	6	0	5	40	62	76	10	0	0	16	28	0	39	12	310
M19	12	5	0	0	50	65	67	10	5	0	12	32	0	56	9	323
M21	9	3	0	0	34	46	98	5	0	0	9	29	0	58	10	301
M22	10	2	0	0	36	56	69	16	4	0	9	33	6	52	8	301
M23	15	4	0	0	36	67	85	12	2	0	8	28	0	39	12	308
M24	16	5	0	6	40	76	61	10	4	6	11	25	0	48	10	318
Mean	14	3	0	2	39	62	79	10	2	1	12	35	1	45	10	314

Qm non – non-undulose monocrystalline quartz; Qm un – undulose monocrystalline quartz; Qp 2-3 – polycrystalline quartzose 2-3 crystal units per grain; Qp >3 – polycrystalline quartzose more than 3 crystal units per grain; K – potassium feldspar; P – plagioclase feldspar; Lv – volcanic rock fragments; Ls – sedimentary rock fragments; Lp – plutonic rock fragments; Lm – metamorphic rock fragments; Cht – chert; M – matrix; Cem – cement; Acc – accessory minerals

tors giving palaeocurrent directions, mainly from planar cross-bedding and imbrication. The measurements then were rotated with respect to the corresponding bedding plane to remove the effects of tectonic tilting. The sandstone hand specimens were cut and thin sections were prepared using standard techniques, to 30 μm thickness (Hutchinson, 1974). Thin sections of 15 sandstone samples were point-counted (n = 300) following the Gazzi-Dickinson method (Ingersoll et al., 1984). Point-counting parameters are listed in Table 2 and the data of recalculated point counting samples are shown in Table 3. The sandstones were classified based on the procedure proposed by Folk (1980). Fifteen sandstone and five shale samples were selected for major oxides geochemical analysis. All samples selected were powdered and homogenized to ensure representative subsampling. An X-ray fluorescence (XRF) spectrometer S4 PIONEER model was used for the determination of the major oxides at the Analytical Center, University of Isfahan, Iran. The incident X-ray beam was produced from a Rh with voltage of 60kV, and a beam current of 150 mA. The level of elemental precision was 0.01%. Loss on ignition (LOI) was determined from the weight loss after roasting the sample at 1000°C for 2 hours. Selected trace elements on six sandstone and four shale samples were analyzed by inductively coupled plasma mass spectrometry (ICP-MS: Agilent series 4500 model at the laboratories of the Zarazma Co., Tehran, Iran). The powdered samples were digested using the multi-acid method at 220°C for four hours and then analyzed. Each analysis was done in duplicate with a reproducibility found to be<±2%. Analyses of standard materials indicate that the results are generally accurate to within ±10%.

RESULTS

STRATIGRAPHY

In this study, the lowermost part of the Akhoreh Formation was measured and logged in the Shurab section, ~20 km north of Nain, east Isfahan (Shurab section: N33°01'47", E53°07'39") the area of the type section for this formation (Davoudzadeh, 1972; Fig. 3). The Middle Eocene to lowermost Oligocene Akhoreh Formation overlies the NOM with a faulted contact and underlain conformably by the Lower Red Formation (Davoudzadeh, 1972; Fig. 3). In the study area, the lowermost part of the Akhoreh Formation is ~500 m thick (Fig. 4). The main lithostratigraphic features seen in the Shurab section are as follows:

The lowermost lithostratigraphic unit (45 m thick) is composed of a well-developed, mostly massive, matrix-supported conglomerate with angular to sub-angular clasts within a pinkish sandy matrix (Table 1 and Fig. 5A, B). The clasts are mainly pebble-sized, of predominantly mafic to ultramafic igneous

Table 3

QFL percentage of the lower Akhoreh sandstones at the Shurab section in the north of Nain, Central Iran

Sample	QmFLt (%)			QtFL(%)			QFR(%)		
	Qm	F	Lt	Qt	F	L	Q	F	R
M1	11	49	40	18	49	33	14	49	37
M2	7	45	48	10	45	46	7	45	48
M4	7	49	44	12	49	39	7	49	44
M6	7	46	47	14	46	40	9	46	45
M7	7	46	47	16	46	38	9	46	45
M8	6	41	53	13	41	46	9	41	50
M9	12	45	44	18	45	37	12	45	44
M11	7	40	53	12	40	47	7	40	53
M13	6	46	49	12	46	42	6	46	49
M14	6	38	56	14	38	48	6	38	56
M16	4	51	45	10	51	40	4	51	45
M17	7	48	44	12	48	40	7	48	44
M18	10	44	46	19	44	37	12	44	44
M19	8	52	40	13	52	35	8	52	40
M21	6	39	55	10	39	50	6	39	55
M22	6	46	47	11	46	43	6	46	47
M23	8	45	46	12	45	43	8	45	46
M24	9	50	41	16	50	33	12	50	38
Mean	7	45	48	13	45	42	8	45	47

Qm – monocrystalline quartz; F – feldspar; L – unstable lithic fragments (Lv + Ls + Lm); Lt – total lithic fragments (L + Qp); R – rock fragments

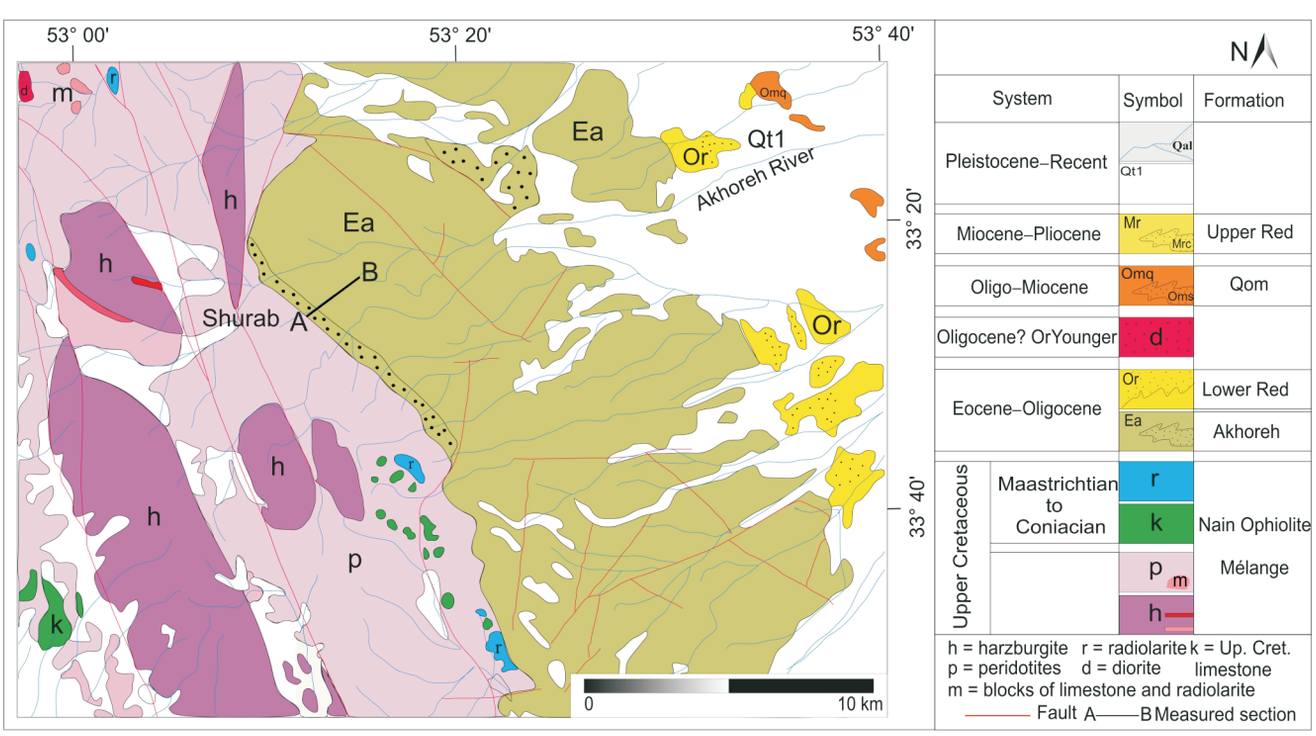

Fig. 3. Geological map of the study area reproduced from a geological map of Nain at the scale of 1:100,000 (modified after Davoudzadeh, 1972)

Locations of the measured stratigraphic sections of the lower Akhoreh Formation are shown (A–B – shurab section)

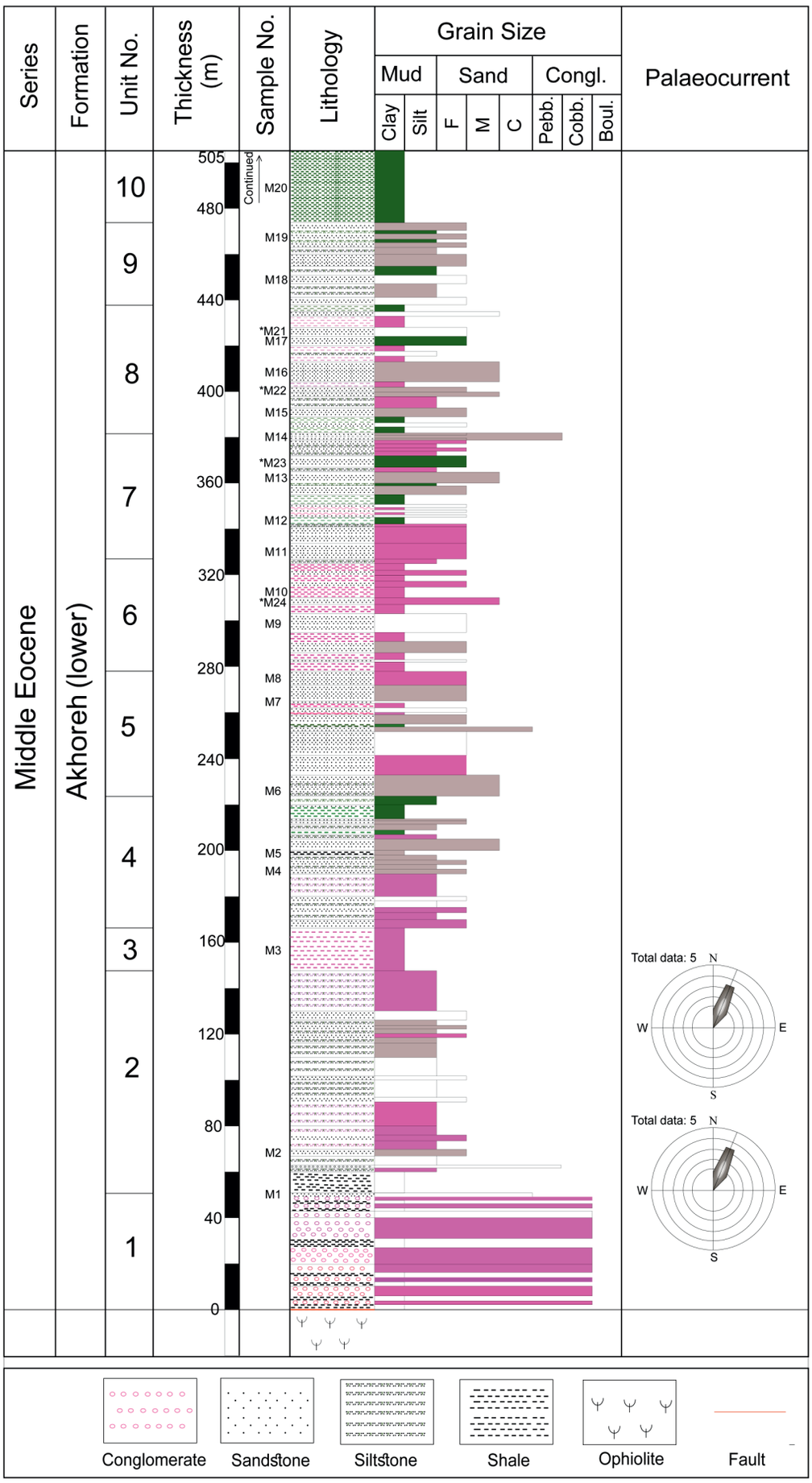

Fig. 4. Lithostratigraphic column of the lower Akhoreh Formation, Shurab section to the north of Nain, Central Iran

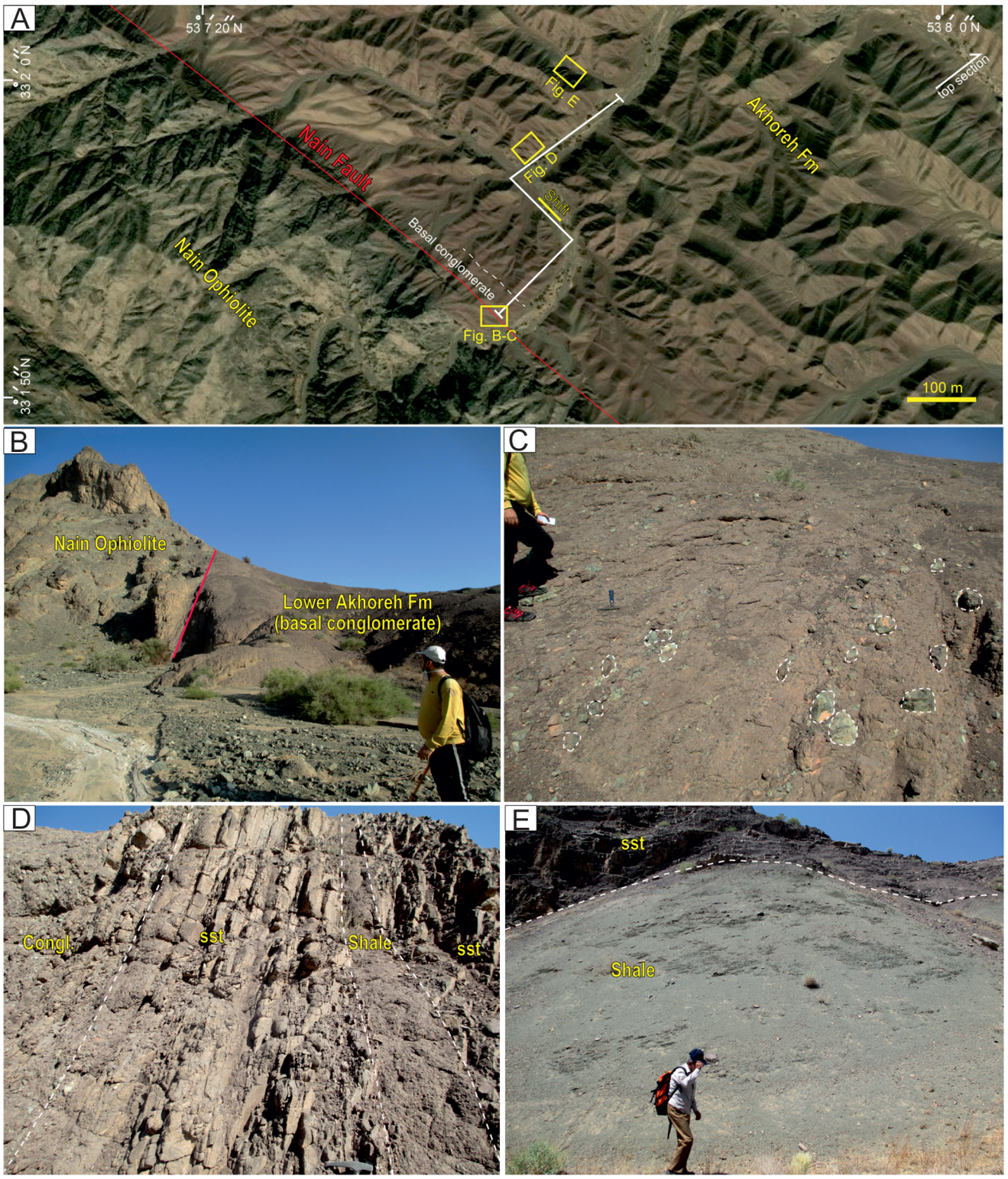

Fig. 5. Overview of satellite image and field photographs of the lower Akhoreh Formation to the north of Nain, Central Iran

A – satellite image of the study area (Shurab section) with the fault boundary between the Nain Ophiolite and the Akhoreh Formation. The traverse line (white) shows the measurement route of the stratigraphic logs. The position of the field photos is shown by rectangles; **B** – an overview of the lower Akhoreh Formation that rests on the NOM with fault contact. View to the north-west; **C** – basal matrix-supported conglomerate with cobble-sized mafic and ultramafic clasts; **D** – red to pink, fine-grained conglomerate, sandstone (sst) and shale intercalations with a general fining-upwards pattern (stratigraphic top is to the right); **E** – thick light green shales

rocks, and rarely are locally-derived boulders up to 50 cm across. This unit fines upwards, changing to a fine-grained conglomerate of average 5 cm clast size (Fig. 5C). The clast compositions include dark green ultrabasic and basic rocks (gabbro, peridotite [harzburgite], serpentinites, basalt and rare white granite) as well as red radiolarian cherts and siliceous limestones. These pebbles and cobbles locally show imbrication indicating palaeocurrents towards the north-north-east. The basal conglomerate is overlain by ~103 m (Unit 2) of sharp-based lenticular pebbly sandstones that grade into pink to red, medium- to thick-bedded sandstones with mud cracks on bedding surfaces as well as pink siltstone and shale intercalations. Mud cracks and the reddish colour of the succession indicate at least subaerial exposure in a continental environment. The succeeding lithostratigraphic unit (Unit 3) consists of red shale and thin siltstone intercalations. Unit 4 is composed of grey siltstones and red shales at the base passing up into pink and grey coarse-grained sandstones with pedogenic fabrics. This unit grades up into green shales. Units 5 and 6 consist of interbedded green shales with pink and grey coarse-grained sandstone showing trough cross-bedding. Unit 7 consists of interbedded green shales with pink horizontally-laminated sandstones. Unit 8 starts with massive matrix-supported conglomerates with a coarse-grained sandy matrix (Fig. 5D). The clasts are pebble-sized and mostly volcanic in composition, from andesitic to basaltic, suggesting a magmatic arc-related provenance. The rest of this unit consists of grey sandstone and pink to green shale intercalations with a general fining-upwards pattern. Unit 9 consists of grey sandstone and siltstone intercalations and subordinate interlayers of green shale. The uppermost part of the measured section in the lower Akhoreh Formation is dominated by relatively thick light green shales (30 m), which are considered as an index unit at the top that is measured in this study from the lower part of the Akhoreh Formation at the type section (Fig. 5E).

PETROGRAPHY

The sandstones of the lower Akhoreh Formation are mostly poorly sorted, immature, medium- to fine-grained. They comprise framework grains such as quartz, feldspar (plagioclase and K-feldspar) and rock fragments (volcanic, sedimentary and metamorphic) together with matrix, cement and accessory minerals (Table 2). Among the quartz grains, monocrystalline quartz is most common (comprising 3–7%) showing mostly a euhedral shape with straight extinction (Fig. 6A and Table 3). The quartz grains are mostly angular to sub-angular, sometimes displaying embayment characteristic of volcanic origin. The feldspar constitutes 30–35% of the framework grains, relatively unweathered plagioclase dominating over K-feldspar (Fig. 6B). The samples also are rich in intermediate to ultramafic, rarely plutonic, more frequently volcanic, rock fragments (avg. 25%). The igneous rock fragments include microlithic and lathwork andesitic to basaltic volcanic lithics; plutonic rock fragments (avg. 1%) range in composition from diorite, gabbro to peridotite (Fig. 6C, D). Other rock fragments include serpentinite (Fig. 6E), microcrystalline chert (avg. 4%; Fig. 6F), radiolarian chert and carbonate (Fig. 6G). Metamorphic rock fragments are rare (<2%). The sandstones contain at least 5% of pseudo- and epi-matrix. These sandstones are generally rich in iron ore (hematite) minerals (2–4%). The common accessory minerals are pyroxenes and red to brown chromian spinels (Fig. 6H, I).

Carbonate (calcite and dolomite) cement commonly lithified the sandstones, likely in the early stages of diagenesis due to the low compaction of the constituent grains.

Modal data plot within the lithic arkose ($Q_8F_{48}L_{44}$) and feldspathic litharenite (volcanic arenite) ($Q_8F_{44}L_{48}$) fields of the QFL ternary diagram (Folk, 1980; Fig. 7). These compositions indicate an arc-related provenance for the lower Akhoreh Formation.

GEOCHEMISTRY

The bulk geochemical composition of selected sandstone and shale samples of the lower Akhoreh Formation are listed in tables 4–6. The major, trace and rare earth element (REE) compositions of the samples are evaluated below.

MAJOR ELEMENTS

The SiO_2 content of the lower Akhoreh sandstones varies between 36.5 and 46.5% (avg. 40.8%), and for shale samples it ranges between 43.0 and 48.3% (avg. 46.7%). The Al_2O_3 content of the sandstones varies between 8.9 and 11% (avg. 10.4%), for shale samples varying between 10.7 and 13.3% (avg. 11.8%). Fe_2O_3, MgO and CaO concentrations of the sandstones (avg. 7.1, 10.2, 15.2%, respectively) and shales (avg. 8.6, 9.8, 9.6%, respectively) are high, while the remaining major oxides (K_2O, Na_2O, TiO_2 and MnO) have low concentrations (avg. <3%; Table 4).

The Low SiO_2/Al_2O_3 content of the sandstone samples indicates immature sandstones with high clay and detrital Al-silicate contents. The lower Akhoreh sandstones, in the major oxide-based diagram for chemical classification of sandstones (Pettijohn et al., 1972), plot in the greywacke field, very close to the lithic arenite field (Fig. 8). The TiO_2 concentration of the samples is similar to the mean composition of the Upper Continental Crust (UCC). Fe_2O_3 and MnO are slightly enriched compared to UCC, while MgO and CaO are strongly enriched in the sandstone samples (Fig. 9A). The P_2O_5, Na_2O, Al_2O_3 and SiO_2 concentrations in the sandstones are slightly depleted compared to UCC, while K_2O is strongly depleted. The shale samples show similar concentrations of P_2O_5, Al_2O_3 and TiO_2 relative to UCC (Fig. 9B). These samples also show enrichment in MgO, CaO, MnO and Fe_2O_3 contents and slight depletion in Na_2O, K_2O and SiO_2 (Fig. 9B).

TRACE AND RARE EARTH ELEMENTS

Some trace elements, such as V, Sc, Co, Ni, Cr, show enrichment in the sandstone and shale samples compared to UCC (Fig. 9C, D), while, Rb, Ba, Zr, Hf, Th, U and Y are depleted relative to UCC. Sr and Rb are similar to UCC values. Elements such as V, Ni, Cr, Sr and Ba (avg. 166.5, 457.7, 837, 383., 176.8 ppm, respectively) have values above 100 ppm, while other elements such as Sc, Co, Rb, Zr, Hf, Th, U, Y and Nb have concentrations of <100 ppm (Table 5). REE concentrations of the samples studied are shown in Table 6. The REE contents of the sandstones studied vary from 46.4 to 83.8 ppm (avg. 63.9 ppm), while those of shale samples vary between 80.0 to 112.0 (avg. 94.4 ppm). Concentrations of light REE (~37.57–71.02 and ~65.96–95.51 ppm in sandstones and shales, respectively) are higher than those of the heavy REEs (~8.86–12.74 ppm in sandstones and ~13.32–16.51 ppm in shales). Chondrite-normalized REE patterns of the Akhoreh

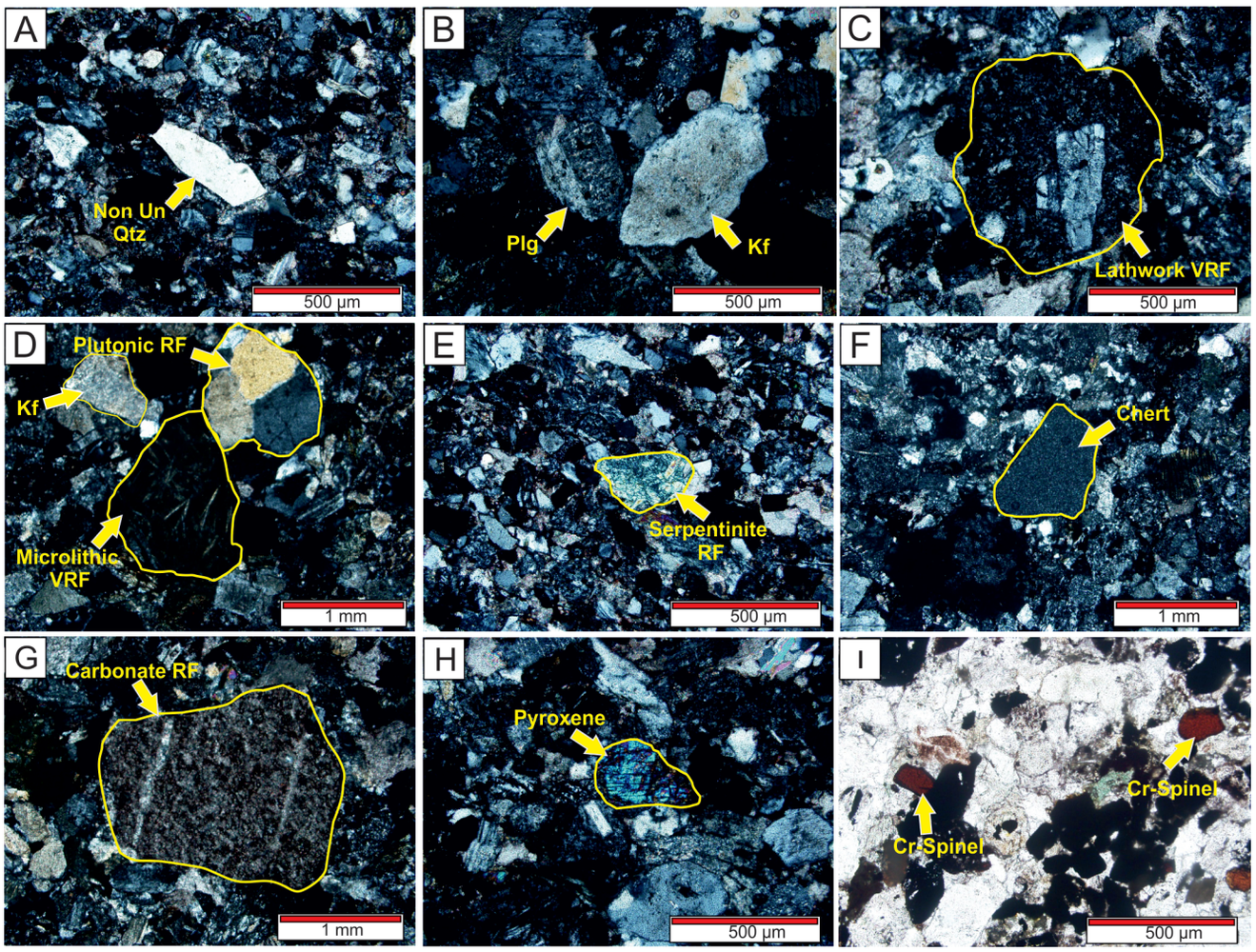

Fig. 6. Representative microphotographs of framework and accessory grains of the lower Akhoreh Formation sandstones of the Shurab section to the north of Nain, Central Iran

A – monocrystalline non-undulose quartz (Non Un Qtz) with euhedral shape and straight extinction; **B** – plagioclase (Plg) with Carlsbad twining and semi-altered K-feldspar (Kf) in a lithic arkose; **C** – volcanic rock fragment (VRF) with lathwork fabric; **D** – volcanic rock fragment with microlithic fabric, plutonic rock fragment and altered K-feldspar (Kf) in a feldspathic litharenite; **E** – serpentinite rock fragment (RF) that indicates ophiolite provenance; **F** – chert fragment; **G** – carbonate rock fragment; **H** – pyroxene heavy mineral; **I** – Cr-spinel of red to brown colour; A–H – crossed polarized light; I – plane polarized light

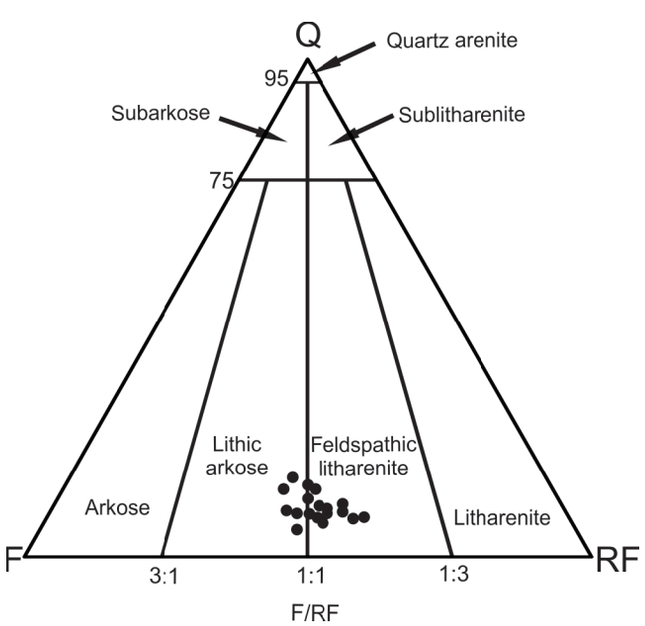

Fig. 7. Classification of the lower Akhoreh sandstones in the ternary plot of Folk (1980)

Q – quartz, F – feldspar, RF – rock fragment

Table 4

Major element concentrations (wt.%) for the sandstone and shale samples from the lower Akhoreh Formation at the Shurab section in the north of Nain, Central Iran

Sample	SiO_2	TiO_2	Al_2O_3	Fe_2O_3	MnO	MgO	CaO	Na_2O	K_2O	P_2O_5	LOI	SUM
M-ss1	39.56	0.51	8.95	8.3	0.14	16.93	13.53	1.12	0.76	0.045	9.47	99.81
M-ss4	40.55	0.53	9.95	6.47	0.14	10.7	16.06	2.44	0.51	0.08	12.07	99.80
M-ss6	40.68	0.60	10.2	6.42	0.15	8.83	17.39	2.64	0.75	0.076	11.76	99.80
M-ss7	43.67	0.53	11.2	5.84	0.12	12.76	11.68	3	0.45	0.068	10.12	99.77
M-ss8	40.63	0.55	10.4	6.83	0.15	11.1	14.84	2.93	0.48	0.068	11.5	99.78
M-ss9	46.49	0.86	10.7	7.51	0.15	8.18	13.29	2.62	1.22	0.097	8.3	99.66
M-ss14	36.49	0.78	10.2	7.78	0.18	13.99	15.01	2.37	0.66	0.069	11.77	99.65
M-ss15	40.81	0.75	10.5	7.79	0.15	9.12	15.5	2.63	0.88	0.081	11.17	99.70
M-ss16	37.84	0.71	10.1	7.03	0.14	8.99	17.61	2.85	0.73	0.07	13.2	99.52
M-ss17	39.89	0.50	11	5.4	0.14	9.89	15.82	3.46	0.90	0.07	12.33	99.15
M-ss18	42.36	0.51	10.9	6.19	0.14	8.9	15.41	2.74	0.99	0.08	11.34	99.65
M-ss19	41.73	0.73	11.5	6.87	0.13	10	13.74	2.96	1.12	0.079	10.53	99.61
M-ss21	38.57	0.70	10.1	8.61	0.13	8.73	15.94	2.95	0.78	0.069	12.55	99.68
M-ss22	41.82	0.58	10.4	7.82	0.16	7.97	16.02	2.54	0.96	0.077	11.05	99.74
M-ss23	41.66	0.60	10.6	7.31	0.15	7.68	16.05	2.8	0.95	0.081	11.51	99.73
Mean	40.85	0.63	10.45	7.08	0.14	10.25	15.19	2.67	0.81	0.07	11.24	99.67
STDV*	2.32	0.11	0.58	0.88	0.01	2.46	1.53	0.49	0.22	0.01	1.20	
M-sh3	47.9	0.65	11	8.93	0.17	10.1	9.93	1.49	2.07	0.14	7.08	99.70
M-sh5	46.87	0.67	11.3	8.55	0.17	8.94	11.74	1.38	2.15	0.15	7.7	99.81
M-sh10	48.33	0.67	12.6	7.87	0.14	8.33	9.43	1.39	2.92	0.014	7.74	99.76
M-sh12	47.57	0.67	13.3	8.37	0.12	9.1	7.55	1.47	2.66	0.15	8.59	99.50
M-sh20	43.03	0.58	10.7	9.33	0.17	12.79	9.23	0.868	1.32	0.13	11.4	99.71
Mean	46.74	0.65	11.78	8.61	0.15	9.85	9.58	1.32	2.22	0.12	8.50	99.70
STDV*	1.92	0.03	1.00	0.50	0.02	1.58	1.35	0.23	0.55	0.05	1.53	

* – standard deviation; ss – sandstones, sh – shales

sandstones and shales are shown in Figure 9E, F. The chondrite-normalized REE patterns of the Akhoreh Formation samples indicate that all samples show LREE-enriched and flat HREE patterns (Fig. 9E, F). The mean value of Eu/Eu* is 0.98 in sandstone and 0.86 in shale samples of the lower Akhoreh Formation.

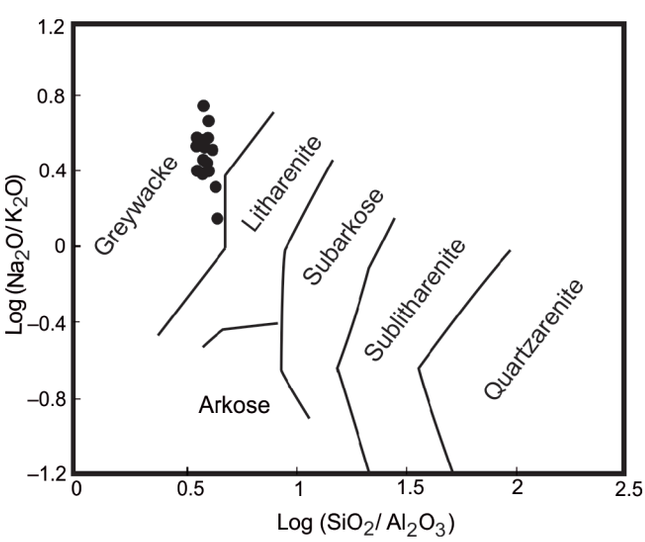

Fig. 8. Chemical classification of the lower Akhoreh sandstones in the diagram of Pettijohn et al. (1972)

DISCUSSION

PETROGRAPHY

Sandstone petrographic studies show that plagioclase feldspar and Igneous rock fragments, along with less frequent quartz, constituent the main framework of the sandstones. Modal analysis led to the identification of two texturally and mineralogically immature petrofacies, including feldspathic litharenite and lithic arkose.

The presence of plagioclase, mafic and ultramafic lithic fragments (i.e., serpentinite), lathwork volcanic lithics, and radiolarite, as well as heavy minerals such as Cr-spinel and clinopyroxene in the lower Akhoreh sandstones, are evidence for dominant mafic-ultramafic source rocks of ophiolitic mélange provenance mixed with continental provenance.

SOURCE AREA WEATHERING

The climatic conditions and palaeoweathering of central Iran during the Middle Eocene was evaluated through modal data of the lower Akhoreh sandstones using discrimination diagrams. Plotting data on a Qp/F+RF *versus* Q/F+RF bivariate diagram (Suttner and Dutta, 1986) indicate arid to semi-arid climatic conditions (Fig. 10A). Suttner and Dutta (1986) proposed a bivariate diagram of SiO_2 *versus* Al_2O_3+K_2O+Na_2O to determine climatic conditions of the source area. This plot revealed a high probability of an arid climate for the Akhoreh Formation sandstones (Fig. 10B).

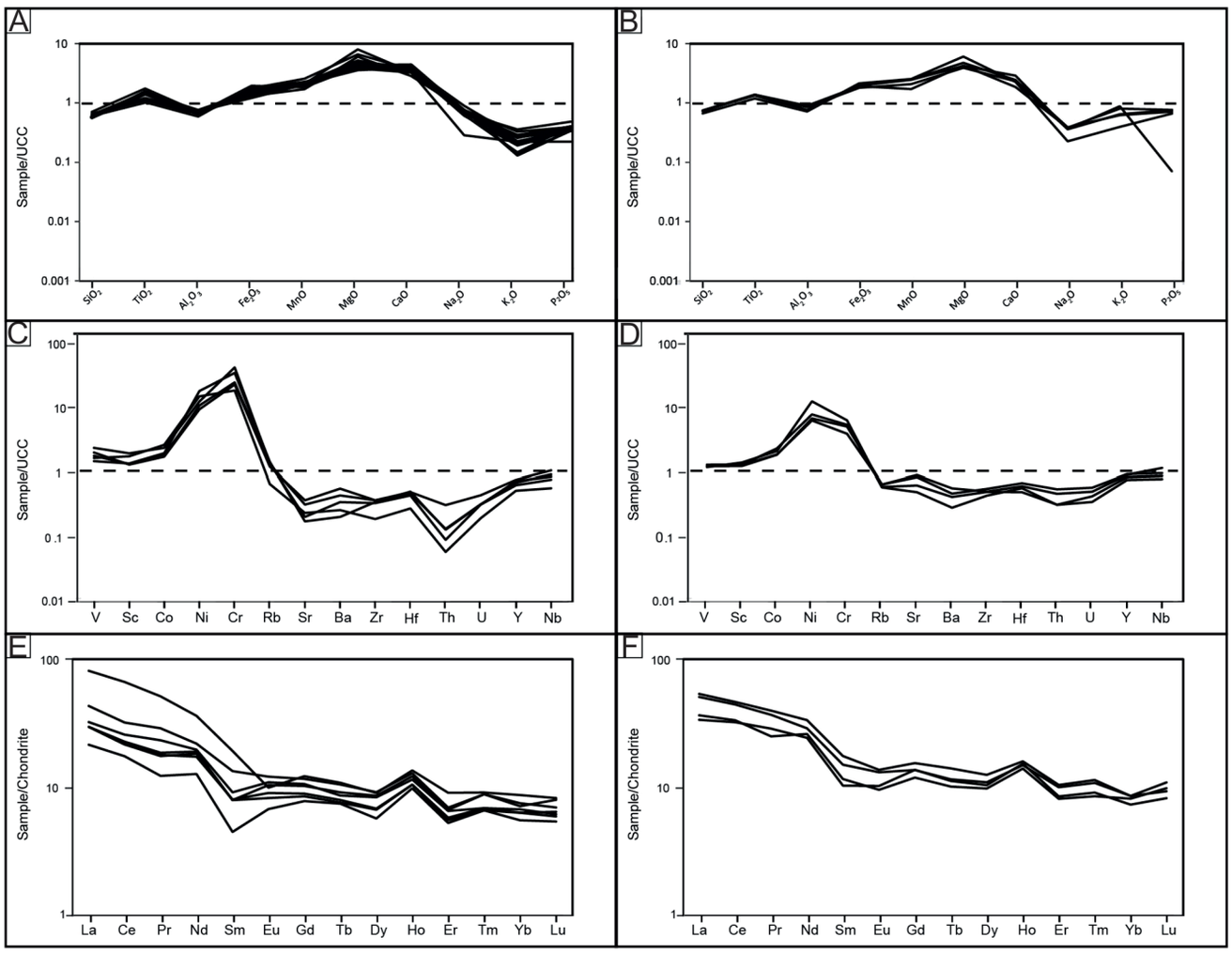

Fig. 9A, B – UCC-normalized major oxides of the lower Akhoreh sandstones (right) and shales (left); C, D – UCC-normalized trace elements of the lower Akhoreh sandstones (right) and shales (left); E, F – chondrite-normalized REE of the lower Akhoreh sandstones (right) and shales (left); UCC and chondrite normalization factors are from Rudnick and Gao (2003)

Table 5

Trace element compositions (in ppm) of the lower Akhoreh sandstone and shale samples at the Shurab section in the north of Nain, Central Iran

Sample	V	Sc	Co	Ni	Cr	Sr	Rb	Ba	Zr	Hf	Th	U	Y	Nb
DL	1	0.5	1	1	1	1	1	1	5	0.5	0.1	0.1	0.5	1
M-ss1	149	20	37	510	493	202.7	24	130	33	1.45	0.6	0.5	10.1	6
M-ss7	133	15.6	27.8	612	907	429.9	18	103	59	2.58	1.29	0.8	12.2	8
M-ss9	179	15	24.7	326	608	363.7	37	271	63	2.54	3.01	1.1	14.6	10.9
M-ss14	211	22.2	33.5	426	1096	405.8	21	171	57	2.27	0.91	0.8	14	8.9
M-ss19	160	15.4	25.9	372	653	395.1	32	215	63	2.44	1.33	0.81	13.3	9.5
M-ss21	167	14.6	27.4	500	1265	501.4	25	171	51	1.95	0.62	0.6	11.9	7.8
Mean	166.5	17.1	29.4	457.7	837.0	383.1	26.2	176.8	54.3	2.2	1.3	0.8	12.7	8.5
STDV*	24.52	2.89	4.39	94.89	276.83	91.07	6.47	54.83	10.37	0.40	0.82	0.19	1.49	1.52
M-sh3	128	16.4	36.4	319	175	193.5	65	212	88	2.65	3.13	1.1	17.1	9.7
M-sh10	121	15.6	29.1	276	164	210.8	93	288	89	3.28	4.61	1.3	18.5	12.8
M-sh12	123	16.1	29.3	256	127	209.7	87	238	98	3.64	5.42	1.5	18.9	10.7
M-sh20	118	17.7	33.2	510	205	189.2	51	144	77	3.05	3.12	0.9	15.5	8.7
Mean	122.5	16.5	32.0	340.3	167.8	200.8	74.0	220.5	88.0	3.2	4.1	1.2	17.5	10.5
STDV*	3.64	0.78	3.02	100.61	27.90	9.58	16.88	51.93	7.45	0.36	0.99	0.22	1.33	1.52

DL – detection limit; * – standard deviation

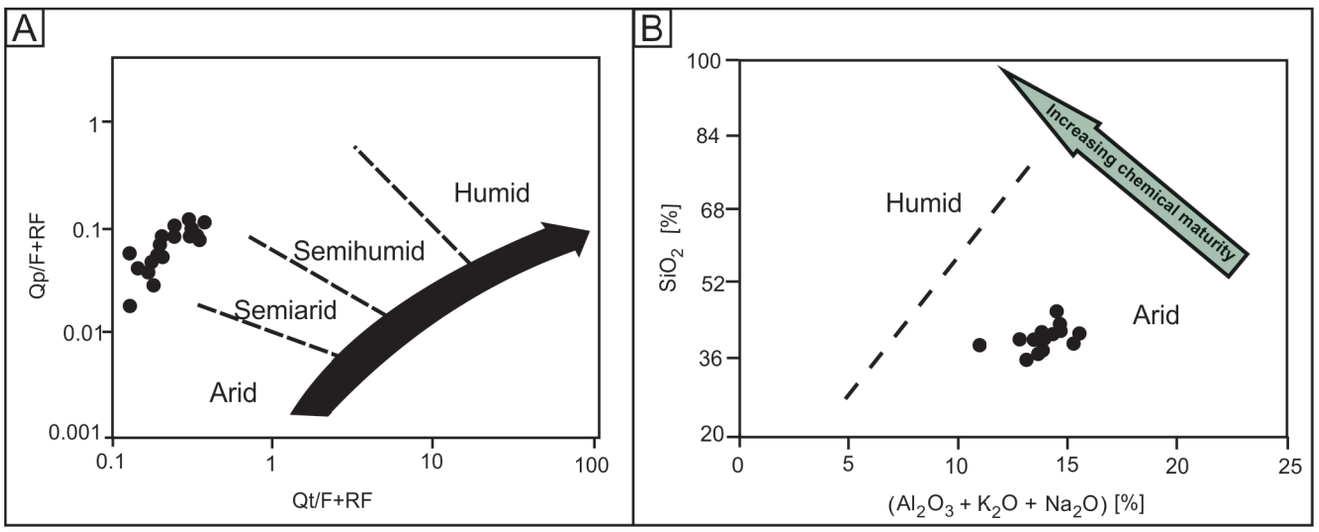

Fig. 10A – climatic condition bivariate discrimination diagram of Qp/F+RF *versus* Q/F+RF for the lower Akhoreh sandstones (after Suttner and Dutta, 1986); B – SiO_2 (wt.%) *versus* (Al_2O_3+K_2O+Na_2O) bivariate diagram for the sandstones of the lower Akhoreh sandstones (after Suttner and Dutta, 1986)

The Chemical Index of Alteration (CIA), introduced by Nesbitt and Young (1982), has been widely used to constrain the degree of weathering in the source area (e.g., Garzanti and Resentini, 2016; Ramos-Vázquez et al., 2022). Higher CIA values (80–100) reflect the removal of labile cations (Na^+, K^+, Ca^{2+}) relative to residual cations (Al^{+3}) and indicate intense weathering in the source terrains, whereas lower values (< 60) represent weaker weathering (Fedo et al., 1995). The CIA is measured via an equation: CIA = [Al_2O_3/(Al_2O_3+CaO*+ Na_2O+K_2O)]*100. All the oxides are in molecular proportion and CaO^* represents Ca in silicate minerals. Quantification of the CaO content (CaO*) of the silicate fraction involves subtraction of the molar proportion of P_2O_5 from the molar proportion of total CaO. After subtraction, if the "remaining number of moles" is found to be less than the molar proportion of Na_2O, then the "remaining number of moles" is considered as the molar proportion of CaO of the silicate fraction. If the "remaining number of moles" is greater than the molar proportion of Na_2O, then the molar proportion of Na_2O is considered as the molar proportion of CaO of the silicate fraction (CaO*).

The CIA value of the lower Akhoreh samples range from 60 to 74 (avg. 63) for the sandstones, indicating weak weathering probably of first cycle sediments and/or short distance transport as well as rapid deposition. The CIA value for the shale samples reaches a higher average (71) pointing to moderate weathering.

Our modal and geochemistry data indicate an arid to semi-arid climate and short-distance transport, and a weak to moderate weathering condition for the lower Akhoreh terrigenous deposits.

Table 6

REE concentration (in ppm) of the lower Akhoreh sandstone and shale samples at the Shurab section in the north of Nain, Central Iran

Sample	La	Ce	Pr	Nd	Sm	Eu	Gd	Tb	Dy	Ho	Er	Tm	Yb	Lu
DL	1	0.5	0.05	1	0.02	0.1	0.05	0.1	0.02	0.05	0.05	0.1	0.05	0.1
M-ss1	8	17	1.71	9.2	1.06	0.6	2.43	0.44	2.22	0.58	1.34	0.24	1.4	0.21
M-ss7	11	21	2.44	13.2	1.87	0.73	2.65	0.45	2.6	0.62	1.47	0.25	1.6	0.25
M-ss9	16	31	4.01	15.8	3.14	1.07	3.62	0.62	3.55	0.76	1.76	0.32	1.8	0.31
M-ss14	11	22	2.59	13.7	1.87	0.92	3.19	0.54	3.34	0.72	1.69	0.32	1.9	0.27
M-ss19	12	25	3.23	14.2	2.15	0.97	3.3	0.51	3.24	0.68	1.66	0.25	1.7	0.24
M-ss21	11	21	2.49	12.50	1.89	0.80	2.78	0.47	2.65	0.62	1.41	0.24	1.60	0.23
Mean	11.50	22.83	2.75	13.10	2.00	0.85	3.00	0.51	2.93	0.66	1.56	0.27	1.67	0.25
STDV*	2.36	4.34	0.72	2.02	0.61	0.16	0.41	0.06	0.47	0.06	0.16	0.04	0.16	0.03
M-sh3	13	31	3.34	18.1	2.64	0.82	3.59	0.58	3.68	0.80	2	0.3	2	0.37
M-sh10	18	41	4.89	20	3.4	1.12	4.1	0.66	4.11	0.85	2.46	0.38	2.1	0.35
M-sh12	19	43	5.27	23.1	3.97	1.17	4.64	0.8	4.69	0.91	2.56	0.4	2.1	0.41
M-sh20	12	30	3.83	16.9	2.35	0.88	4.12	0.64	3.91	0.87	2.09	0.32	1.8	0.31
Mean	15.50	36.25	4.33	19.53	3.09	1.00	4.11	0.67	4.10	0.86	2.28	0.35	2.00	0.36
STDV*	3.04	5.80	0.78	2.34	0.64	0.15	0.37	0.08	0.37	0.04	0.24	0.04	0.12	0.04

DL – detection limit; * – standard deviation

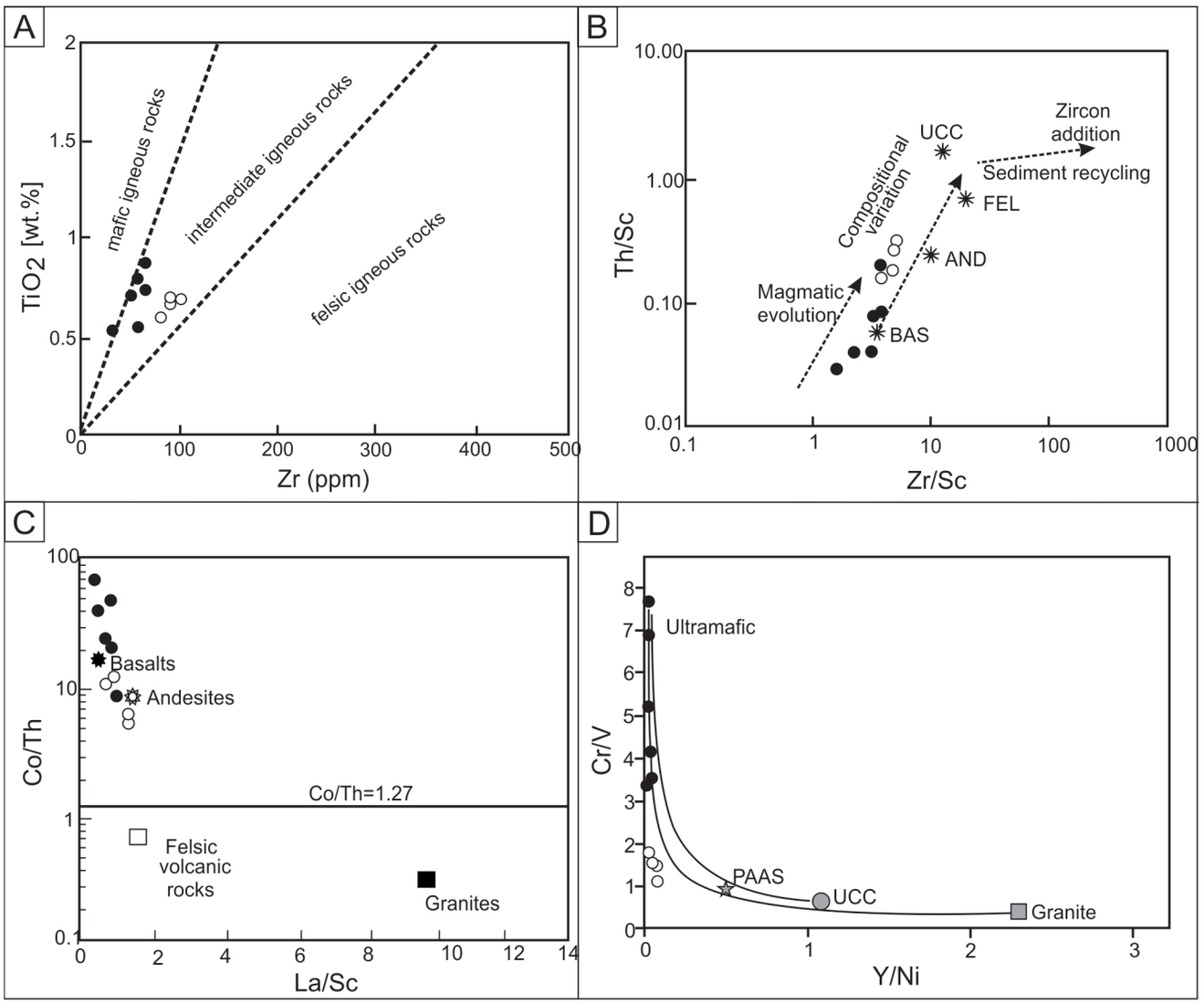

Fig. 11. Source rock composition discrimination diagrams of the lower Akhoreh sandstone and shale samples

A – bivariate diagram of TiO_2 *versus* Zr (after Hayashi et al., 1997); **B** – Th/Sc *versus* Zr/Sc diagram (McLennan et al., 1983); **C** – Co/Th *versus* La/Sc diagram (Gu et al., 2002); **D** – bivariate diagram of Cr/V *versus* Y/Ni (after McLennan et al., 1993); solid circles are sandstone and empty circles are shale samples; FEL – felsic, AND – andesit, BAS – basalt, PAAS – post-Archaean Australian shale, UCC – upper continental crust

SOURCE ROCK COMPOSITION

The constituents of sandstones can indicate the type of lithology of their parent rock (Critelli et al., 1997; Marsaglia et al., 2016; Affolter and Ingersoll, 2019). The volcanic origin of the samples studied is shown by the presence of small amounts of monocrystalline quartz grains that have properties such as crystalline shape, embayments and straight extinction (Ulmer-Scholle et al., 2015), and the values obtained for the plagioclase to total feldspar ratio (Dickinson, 1970). Given the large content of microlithic and lathwork volcanic rock fragments, intermediate to basic volcanic parent rocks, are the main sources for these sandstones. However, the scarce serpentinite rock fragments and the presence of Cr-spinel in the samples studied are evidence of an ophiolite source (Fig. 6E, I). The low amount of both sedimentary and metamorphic rock fragments in the sandstones studied suggests a minor sedimentary and metamorphic source terrain.

Along with the modal analysis, the geochemistry of siliciclastic rocks is widely used to determine the source rock composition (McLennan et al., 1993; Armstrong-Altrin et al., 2015; Taheri et al., 2018; Ramos-Vázquez and Armstrong-Altrin, 2019; Pourdivanbeigi Moghaddam et al., 2020; Armstrong-Altrin et al., 2022).

The lower Akhoreh samples in a major oxide (TiO_2) *versus* trace element (Zr) bivariate diagram (Hayashi et al., 1997) shows sandstones plotting in mafic igneous and shales in intermediate igneous rock provenances (Fig. 11A). The plotted samples on a Th/Sc *versus* Zr/Sc diagram (McLennan et al., 1983) display the same provenances for the sandstones and shales and showed very low enrichment in Zr, probably due to low sediment recycling (Fig. 11B). The samples plotted on a Co/Th *versus* La/Sc diagram (Gu et al., 2002) show that the sandstones and shales plot near the basalt and andesite average compositions, respectively (Fig. 11C). The Cr/V *versus* Y/Ni bivariate diagram was also used to discriminate provenance (McLennan et al., 1993; Fig. 11D). The samples show Cr enrichment and plot near ultramafic sources.

Ratios such as Eu/Eu*, (La/Lu)cn, La/Sc, La/Co, Th/Sc, Th/Co, and Cr/Th are commonly used to determine the provenance composition of a source region because REE, Th and La abundances are higher in felsic rocks than in mafic rocks,

Table 7

Range of elemental ratios of sandstone and shale in this study compared to the ratios in sediments derived from felsic and mafic rocks

Elemental ratio	Sandstones (this study)	Shales (this study)	Range of sediments from felsic sources*	Range of sediments from mafic sources*
Eu/Eu*	0.97–1.15	0.81–0.92	0.40–0.94	0.71–0.95
$(La/Lu)_{cn}$	3.95–5.36	3.65–5.34	3.00–27.0	1.10–7.00
La/Sc	0.40–1.07	0.68–1.18	2.50–16.3	0.43–0.86
La/Co	0.22–0.65	0.36–0.65	1.80–13.8	0.14–0.38
Th/Sc	0.03–0.20	0.18–0.34	0.84–20.5	0.05–0.22
Th/Co	0.02–0.12	0.09–0.18	0.67–19.4	0.04–1.40
Cr/Th	201–2040	23.4–65.7	4.00–15.0	25–500

* Cullers (2000); Cullers and Podkovyrov (2000)

whereas the Co, Sc and Cr contents are higher in mafic rocks than in felsic rocks (Cullers, 2000; Armstrong-Altrin et al., 2009). Table 7 shows the values of these ratios in the samples studied compared with those of sediments derived from mafic and felsic rocks. Based on this table, the Eu/Eu*, $(La/Lu)_{cn}$, La/Sc, La/Co, Th/Sc, Th/Co, and Cr/Th ratios of the sandstone and shale samples of the lower Akhoreh Formation fall within the range of sediments derived from mafic source rocks. The Eu/Eu* ratios of the samples are also within the range of peridotites of the NOM (0.77–1.07) reported by Shirdashtzadeh et al. (2014).

TECTONIC SETTING

The tectonic setting of source terrains is one of the important factors which control the detrital and geochemical composition of siliciclastic rocks and sediments (Dickinson et al., 1983; Dickinson, 1985; Roser and Korsch, 1986; Armstrong-Altrin et al., 2015). To investigate the relationship between the modal composition of the sandstones studied and the tectonic setting of the source area, the sandstones of the lower Akhoreh Formation plot in undissected and transitional magmatic arc fields of the Qm-F-Lt and Qt-F-L ternary discrimination diagram of Dickinson (1985; Fig. 12). The arc-related provenance character of the lower Akhoreh samples is evident by volcanic rock fragments and plagioclase-rich sandstones and less frequent plutonic quartz and K-feldspar grains that form the feldspathic and volcanic lithic arenites. Such sandstone petrofacies, predominantly the volcanic lithic arenite, could have been derived from the undissected magmatic arc and then deposited within fore-, back- and intra arc basins (Boggs, 2009). Moreover, the sandstones are poorly sorted and matrix-rich which suggest a nearby source. The UDMA and NOM in the western corner of the CEIM are the main possible source area for the lower Akhoreh Formation.

Recently, bulk rock geochemistry of the sandstone and shale samples has been widely used in different discrimination diagrams for tectonic setting evaluation (Purevjav and Roser, 2013; Zaid, 2015; Ghaznavi et al., 2018; Hashemi Azizi et al., 2018). The geochemical data of the low-silica samples of the lower Akhoreh Formation, plotted on a major oxide-based multi-dimensional tectonic discrimination diagram (Verma and Armstrong-Altrin, 2013), indicating an arc setting for the sand-

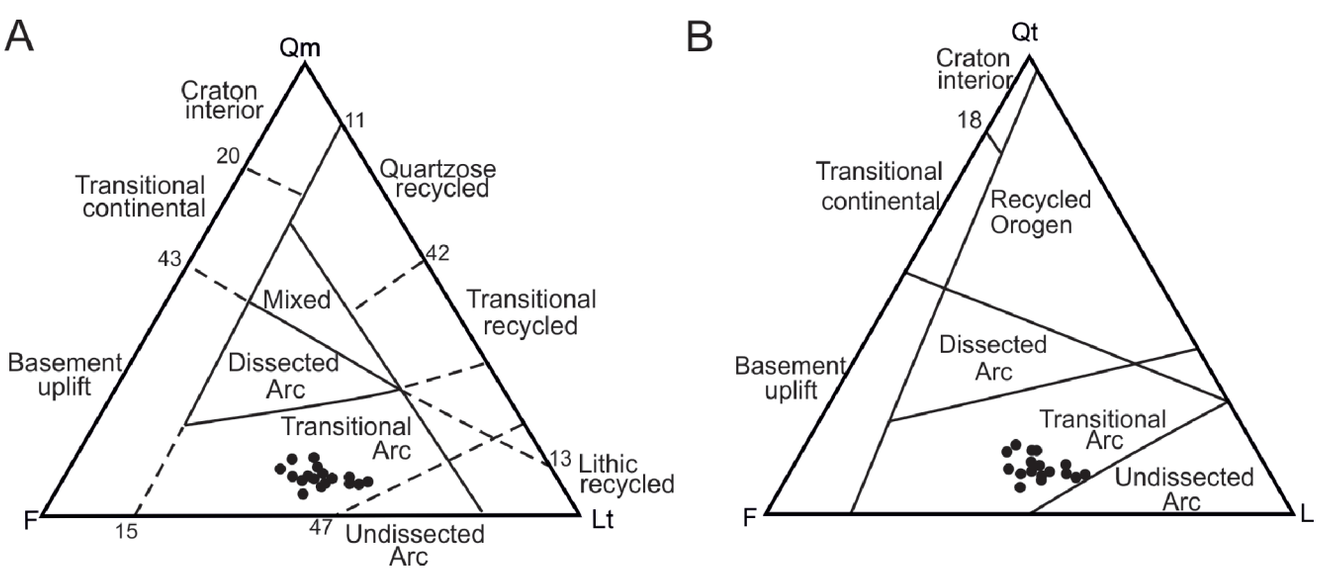

Fig. 12. Provenance discrimination diagrams of the lower Akhoreh sandstones in the ternary plot (A – Qm-F-Lt; B – Qt-F-L; Dickinson, 1985)

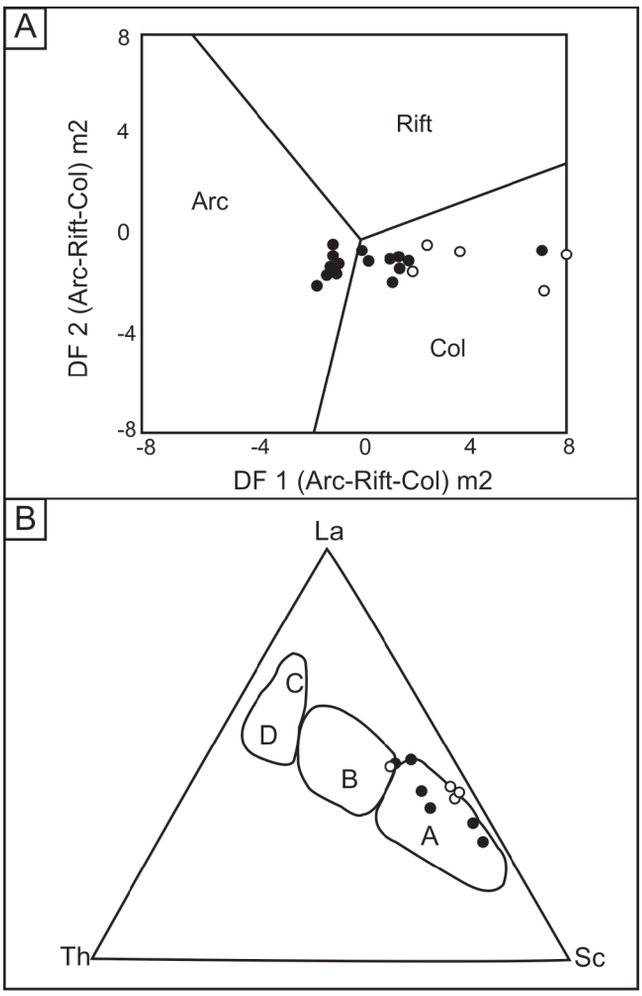

Fig. 13. Tectonic discrimination diagrams of the lower Akhoreh sandstone and shale samples

A – major element-based multidimensional tectonic discrimination function diagram for low-silica samples (Verma and Armstrong-Altrin, 2013); the discriminant function equations are: $DF1_{(Arc\text{-}Rift\text{-}Col)m1}$ = (-0.263 × $ln(TiO_2/SiO_2)_{adj}$) + (0.604 × $ln(Al_2O_3/SiO_2)_{adj}$) + (-1.725 × $ln(Fe_2O_{3t}/SiO_2)_{adj}$) + (0.660 × $ln(MnO/SiO_2)_{adj}$) + (2.191 × $ln(MgO/SiO_2)_{adj}$) + (0.144 × $ln(CaO/SiO_2)_{adj}$) + (-1.304 × $ln(Na_2O/SiO_2)$adj) + (0.054 × $ln(K_2O/SiO_2)_{adj}$) + (-0.330 × ln $(P_2O_5/SiO_2)_{adj}$) + 1 0.588 $DF2_{(Arc\text{-}Rift\text{-}Col)m1}$ = (-1.196 × $ln(TiO_2/SiO_2)_{adj}$) + (1.604 × $ln(Al_2O_3/SiO_2)_{adj}$) + (0.303 × $ln(Fe2O_{3t}/SiO_2)_{adj}$) + (0.436 × $ln(MnO/SiO_2)_{adj}$) + (0.838 × $ln(MgO/SiO_2)_{adj}$) + (-0.407 × $ln(CaO/SiO_2)_{adj}$) + (1.021 × $ln(Na_2O/SiO_2)_{adj}$) + (-1.706 × $ln(K_2O/SiO_2)_{adj}$) + (-0.126 × $ln(P_2O5/SiO_2)_{adj}$) - 1.068; **B** – ternary diagram of La-Th-Sc (Bhatia and Crook, 1986); PM – passive margin, ACM – active continental margin, Col – collision, A – oceanic island arc, B – continental island arc, C – active continental margin, D – passive margin

stone samples and a collisional setting for the shale samples (Fig. 13A). The scatter of the data in this diagram may be related the enrichment of MgO and Fe_2O_3 due to formation of a diagenetic phase such as dolomite cement and the presence of iron-rich heavy minerals in the samples.

Some trace element-based discrimination diagrams that differentiate the type of island arc setting have been used. Trace element geochemical data, on ternary diagrams of La-Th-Sc, plot within the oceanic island arc field (Bhatia and Crook, 1986; Fig. 13B).

REE distribution in clastic sediments can also be used to determine tectonic environments (Bhatia, 1985; McLennan et al., 1993). In the present study, low total REE abundance, slight enrichment of LREE over HREE, and the absence of a negative Eu anomaly on chondrite-normalized plots may suggest an oceanic island arc setting (Table 8).

PALAEOGEOGRAPHIC IMPLICATIONS

Ophiolite mélange, including the NOM, within confining faults of the CEIM during the Late Cretaceous, and a magmatic flare-up of the UDMA in the southwestern margin of the Iran Plate during the Paleogene (Verdel et al., 2011; Mouthereau et al., 2012), played an important role in the Middle Eocene sedimentary provenance of the western corner of CEIM. The obtained results from field, petrographic and geochemical studies of the lower Akhoreh Formation indicate such potential source areas. The lower Akhoreh Formation, that currently lies close to the Nain–Baft transcurrent basin boundary fault, was mostly deposited in non-marine alluvial to fluvial environments (Mallah et al., 2022). The basal conglomerates of the Akhoreh Formation represent angular to sub-angular pebbles and rarely boulders of predominantly ultramafic to mafic igneous rocks such as peridotites, basalts and serpentinite, as well as radiolarian cherts, that were deposited in an alluvial system, where upland streams eroded adjacent highlands of the NOM. The uplift mechanism for the source area may have been triggered by counterclockwise rotation of the CEIM along the Nain–Baft Fault zone after the Late Cretaceous to Middle Eocene (Pirnia et al., 2013; Mattei et al., 2015; Tadayon et al., 2017, 2019). The matrix-rich and poorly sorted texturally and mineralogically immature sandstones (litharenites) also indicate the rapid deposition in continuously subsiding basin. Moreover, the imbrication of clasts in the basal conglomerates as well as other directional sedimentary structures in the sandstones suggest unidirectional palaeocurrents from southwest to the northeast, consistent with the location of the potential source areas.

Based on modal analysis of the sandstones, an arc-related provenance (undissected to transitional arc) is evident in the lowermost Akhoreh Formation from the presence of abundant plagioclase and lithic volcanic fragments (Fig. 12). The geochemistry of the lower Akhoreh samples also suggests an oceanic magmatic arc setting. Although, this tectonic setting generally indicates basic igneous source rocks, the discrimination diagrams of source rock composition show derivation from ultramafic to mafic rocks for the sandstones and mostly intermediate rocks for the shale samples. Based on these different source rock compositions, the fine-grained clastic rocks of the lower Akhoreh Formation most probably have been mainly sourced from intermediate source rocks such as a continental arc like the UDMA. This suggests contribution from the UDMA with calc-alkaline geochemical affinity in addition to the Late Cretaceous NOM (~99 Ma) and relatively more distant pre-Middle Eocene UDMA (40 Ma) in the source region (Shafaii Moghadam et al., 2009; Chiu et al., 2013).

The Lutetian reconstruction of the Iran Plate placed this area at a subtropical palaeolatitude of ~30° north with an arid palaeoclimate (Barrier et al., 2018; Fig. 2). From field studies, and modal and geochemical analysis, the source area had a semi-arid to arid climate. Field evidence such as the reddish sandy matrix of conglomerates, red to pinkish colour of overlying sandstones and shales with some desiccation cracks on bedding surfaces, as well as an absence of plant debris, are indications for an arid palaeoclimate in the western corner of the

Table 8

Comparison of REE characteristics of representative sandstones from different tectonic settings and lower Akhoreh Formation samples

Provenance type	La/Yb	La_N/Yb_N	Eu/Eu*	REE	Tectonic setting
Un-dissected magmatic arc	4.2±1.3	2.8±0.9	1.04±0.11	58±10	Oceanic island arc*
Dissected magmatic arc	11±4	7.5±2.5	0.79±0.13	146±20	Continental island arc*
Uplifted basement	12.5	8.5	0.6	186	Active continental margin*
Craton interior	15.9	10.8	0.56	210	Passive continental margin*
Lower Akhoreh sandstones	6.87	4.64	0.98	63.8	OIA
Lower Akhoreh shales	7.70	5.20	0.86	94.4	OIA

* in the upper right means data from Bhatia and Crook (1986)

CEIM during the Middle Eocene. An arc-related provenance, though, shows little climatic effect due to rapid erosion and a nearby source (Boggs, 2009). The presence of unaltered feldspars and volcanic rock fragments, as well as carbonate rock lithics within the sandstones of the lower Akhoreh Formation, also point to an arid climate. Furthermore, the intensity of the weathering in the source area was low for sandstones to medium for shales by calculating the chemical index of alteration.

Thus, investigation of the palaeogeography of central Iran, as well as field, petrographic and geochemical studies, point out that the NOM, along with the UDMA, having contributed much sediment to the lower Akhoreh Formation, in a local retroarc basin of the CIM and CEIM, by NE-wards flowing rivers in an arid climate, during the Middle Eocene.

CONCLUSIONS

The Middle Eocene lower Akhoreh Formation in its type area in the western corner of the CEIM consists of well-developed conglomerates at the base overlain by an alternation of mostly red to pinkish sandstones and shales.

According to the sandstone petrographic studies, plagioclase feldspars and rock fragments, along with less frequent quartz, constituent the main framework of the sandstones. Igneous rock fragments are more frequent and are predominantly of mafic volcanics. Modal analysis led to the identification of two texturally and mineralogically immature petrofacies, including feldspathic litharenite and lithic arkose.

The normalized geochemical composition of the samples studied compared to the UCC and chondrite indicates a high content of MgO, Ni and Cr and Cr/V, indicating an ultramafic to mafic source rock composition such as ophiolite sources.

Based on the model analysis, the high proportion of plagioclase and rock fragments indicate an arc-related provenance within a transitional to undissected arc tectonic setting. Geochemical analysis (major and trace elements) shows derivation from ultramafic to mafic igneous rocks for the sandstones and mostly intermediate igneous rocks for the shales in an oceanic magmatic arc tectonic setting.

According to the results of modal and geochemical analysis, the source area had an arid climate. Moreover, the CIA average values for sandstones (63) and shales (71) indicate that the intensity of weathering in the source area was low and medium, respectively.

Generally, field, petrographic and geochemical studies indicate that the NOM, along with the UDMA in the west, has contributed major sediment to the lower Akhoreh Formation in a local retroarc basin of the western corner of the CEIM, via rivers flowing from southwest to northeast in an arid climate during the Middle Eocene.

Acknowledgements. This research was supported by the Department of Geology, University of Isfahan, Iran. We thank Meisam Tadayon (Isfahan) for valuable comments, suggestions and revision of the manuscript. Constructive reviews by John Armstrong-Altrin (Ciudad de México), Patrycja Wójcik-Tabol (Kraków) and Sanjeet Kumar Verma (San Luis Potosí) are gratefully acknowledged.

REFERENCES

Affolter, M.D., Ingersoll, R.V., 2019. Quantitative analysis of volcanic lithic fragments. Journal of Sedimentary Research, **89**: 479–486; https://doi.org/10.2110/jsr.2019.30

Agard, P., Omrani, J., Jolivet, L., Whitechurch, H., Vrielynck, B., Spakman, W., Monie, P., Meyer, B., Wortel, R., 2011. Zagros orogeny: a subduction-dominated process. Geological Magazine, **148**: 692–725; https://doi.org/10.1017/S001675681100046X

Allen, M., Jackson, J., Walker, R., 2004. Late Cenozoic reorganization of the Arabia-Eurasia collision and the comparison of short-term and long-term deformation rates. Tectonics, **23**: TC2008; https://doi.org/10.1029/2003TC001530

Armstrong-Altrin, J.S., 2009. Provenance of sands from Cazones, Acapulco, and Bahía Kino beaches, México. Revista Mexicana Ciencias Geológicas, **26**: 764–782.

Armstrong-Altrin, J.S., 2020. Detrital zircon U–Pb geochronology and geochemistry of the Riachuelos and Palma Sola beach sediments, Veracruz State, Gulf of Mexico: a new insight on palaeoenvironment. Journal of Palaeogeography, **9**: 1–28; https://doi.org/10.1186/s42501-020-00075-9

Armstrong-Altrin, J.S., Nagarajan, R., Balaram, V., Natalhy-Pineda, O., 2015. Petrography and geochemistry of sands from the Chachalacas and Veracruz beach areas, western Gulf of Mexico, Mexico: Constraints on provenance and tectonic setting. Journal of South American Earth Sciences, **64**: 199–216; https://doi.org/10.1016/j.jsames.2015.10.012

Armstrong-Altrin, J.S., Madhavaraju, J., Vega-Bautista, F., Ramos-Vázquez, M.A., Pérez-Alvarado, B.Y., Kasper-Zubillaga, J.J., Bessa, A.Z.E., 2021. Mineralogy and geochemistry of Tecolutla and Coatzacoalcos beach sediments, SW Gulf of Mexico. Applied Geochemistry, **134**: 105103; https://doi.org/10.1016/j.apgeochem.2021.105103

Armstrong-Altrin, J.S., Ramos-Vázquez, M.A., Madhavaraju, J., Marca-Castillo, M.E., Machain-Castillo, M.L. Márquez-García, A.Z., 2022. Geochemistry of marine sediments adjacent to the Los Tuxtlas Volcanic Complex, Gulf of Mexico: constraints on weathering and provenance. Applied Geochemistry, **141**: 105321; https://doi.org/10.1016/j.apgeochem.2022.105321

Barrier, E., Vrielynck, B., Brouillet, J.-F., Brunet, M.-F., eds., 2018. Palaeotectonic reconstruction of the central Tethyan realms. Paris, Commission for the Geological Map of the World; CGMW/CCGM.

Basu, A., Bickford, M.E., Deasy, R., 2016. Inferring tectonic provenance of siliciclastic rocks from their chemical compositions: a dissent. Sedimentary Geology, **336**: 26–35; https://doi.org/10.1016/j.sedgeo.2015.11.013

Bhatia, M.R., 1985. Rare earth element geochemistry of Australian Paleozoic graywackes and mudrocks: provenance and tectonic control. Sedimentary Geology, **45**: 97–113; https://doi.org/10.1016/0037-0738(85)90025-9

Bhatia, M.R., Crook, K.A.W., 1986. Trace element characteristics of greywackes and tectonic setting discrimination of sedimentary basins. Contributions to Mineralogy and Petrology, **92**: 181–193; https://doi.org/10.1007/BF00375292

Boggs, S., 2009. Petrology of Sedimentary Rocks. Cambridge University Press, Cambridge.

Chiu, H.-Y., Chung, S.-L., Zarrinkoub, M.H., Mohammadi, S.S., Khatib, M.M., Iizuka, Y., 2013. Zircon U–Pb age constraints from Iran on the magmatic evolution related to Neotethyan subduction and Zagros orogeny. Lithos, **162**–**163**: 70–87; https://doi.org/10.1016/j.lithos.2013.01.006

Critelli, S., 2018. Provenance of Mesozoic to Cenozoic circum-Mediterranean sandstones in relation to tectonic setting. Earth-Science Reviews, **185**: 624–648; https://doi.org/10.1016/j.earscirev.2018.07.001

Critelli, S., Pera, E., Ingersoll, R.V., 1997. The effects of source lithology, transport, deposition and sampling scale on the composition of southern California sand. Sedimentology, **44**: 653–671; https://doi.org/10.1046/j.1365-3091.1997.d01-42.x

Cullers, R.L., 2000. The geochemistry of shales, siltstones and sandstones of Pennsylvanian-Permian age, Colorado, USA: implications for provenance and metamorphic studies. Lithos, **51**: 181–203; https://doi.org/10.1016/S0024-4937(99)00063-8

Cullers, R.L., Podkovyrov, V.N., 2000. Geochemistry of the Mesoproterozoic Lakhanda shales in southeastern Yakutia, Russia: Implications for mineralogical and provenance control, and recycling. Precambrian Research, **104**: 77–93; https://doi.org/10.1016/S0301-9268(00)00090-5

Davoudzadeh, M., 1969. Geologie und Petrographie des Gebietes nördlich von Nain, Zentral-Iran. Ph.D. Thesis, Eidgenossischen Technischen Hochschule (ETH), Zurich.

Davoudzadeh, M., 1972. Geology and petrography of the area north of Nain, central-Iran. Geological Survey of Iran, **14**.

Davoudzadeh, M., Lammerer, B., Weber-Diefenbach, K., 1997. Paleogeography, stratigraphy, and tectonics of the Tertiary of Iran. Neues Jahrbuch für Geologie und Paläontologie Abhandlungen, **205**: 33–67; https://doi.org/10.1127/njgpa/205/1997/33

Dickinson, W.R., 1970. Interpreting detrital modes of graywacke and arkose. Journal of Sedimentary Petrology, **40**: 695–707; https://doi.org/10.1306/74D72018-2B21-11D7-8648000102C1865D

Dickinson, W.R., 1985. Interpreting provenance relation from detrital modes of sandstones. In: Provenance of Arenites (ed. G.G. Zuffa): 333–363. Dordrecht, Reidel Publishing Company; https://doi.org/10.1007/978-94-017-2809-6_15

Dickinson, W.R., Beard, L.S., Brakenridge, G.R., Erjavec, J.L., R.C., F., Inman, K.F., Knepp, R.A., Lindberg, F.A., Ryberg, P.T., 1983. Provenance of North American Phanerozoic sandstones in relation to tectonic setting. GSA Bulletin, **94**: 222–235; https://doi.org/10.1130/0016-7606(1983)94<222:PONAPS>2.0.CO;2

Fedo, C.M., Wayne Nesbitt, H., Young, G.M., 1995. Unraveling the effects of potassium metasomatism in sedimentary rocks and paleosols, with implications for paleoweathering conditions and provenance. Geology, **23**: 921–924; https://doi.org/10.1130/0091-7613(1995)023<0921:UTEOPM>2.3.CO;2

Folk, R.L., 1980. Petrology of Sedimentary Rocks. Hemphill Publishing, Austin, Texas.

Garzanti, E., Resentini, A., 2016. Provenance control on chemical indices of weathering (Taiwan river sands). Sedimentary Geology, **336**: 81–95; https://doi.org/10.1016/j.sedgeo.2015.06.013

Garzanti, E., Andò, S., Scutellŕ, M., 2000. Actualistic ophiolite provenance: The Cyprus Case. The Journal of Geology, **108**: 199–218; https://doi.org/10.1086/314391

Garzanti, E., Vezzoli, G., Andò, S., 2002. Modern sand from obducted ophiolite belts (Sultanate of Oman and United Arab Emirates). The Journal of Geology, **110**: 371–391; https://doi.org/10.1086/340440

Ghaznavi, A.A., Khan, I., Quasim, M.A., Ahmad, A.H.M., 2018. Provenance, tectonic setting, source weathering and palaeoenvironmental implications of Middle-Upper Jurassic rocks of Ler dome, Kachchh, western India:iInferences from petrography and geochemistry. Geochemistry, **78**: 356–371; https://doi.org/10.1016/j.chemer.2018.06.002

Gholami-Zadeh, P., Adabi, M.H., Hisada, K.-i., Hosseini-Barzi, M., Sadeghi, A., Ghassemi, M.R., 2017. Revised version of the Cenozoic collision along the Zagros Orogen, insights from Cr-spinel and sandstone modal analyses. Scientific Reports, **7**: 10828; https://doi.org/10.1038/s41598-017-11042-1

Gu, X.X., Liu, J.M., Zheng, M.H., Tang, J.X., Qi, L., 2002. Provenance and tectonic setting of the Proterozoic turbidites in Hunan, south China: geochemical evidence: Journal of Sedimentary Research, **72**: 393–407; https://doi.org/10.1306/081601720393

Hashemi Azizi, S.H., Rezaee, P., Jafarzadeh, M., Meinhold, G., Moussavi Harami, S.R., Masoodi, M., 2018. Early Mesozoic sedimentary?tectonic evolution of the Central-East Iranian Microcontinent: Evidence from a provenance study of the Nakhlak Group. Geochemistry (Chemie der Erde), **78**: 340–355; https://doi.org/10.1016/j.chemer.2018.06.003

Hassanzadeh, J., Wernicke, B.P., 2016. The Neotethyan Sanandaj-Sirjan zone of Iran as an archetype for passive margin-arc transitions. Tectonics, **35**: 586–621; https://doi.org/10.1002/2015TC003926

Hayashi, K.-I., Fujisawa, H., Holland, H.D., Ohmoto, H., 1997. Geochemistry of ~1.9 Ga sedimentary rocks from northeastern Labrador, Canada. Geochimica et Cosmochimica Acta, **61**: 4115–4137; https://doi.org/10.1016/S0016-7037(97)00214-7

Hutchinson, C.S., 1974. Laboratory Handbook of Petrography Techniques. Wiley, New York.

Ingersoll, R.V., Fullard, T.F., Ford, R.L., Grimm, J.P., Pickle, J.D., Sares, S.W., 1984. The effect of grain size on detrital modes; a test of the Gazzi-Dickinson point-counting method. Journal of Sedimentary Petrology, **54**: 103–116; https://doi.org/10.1306/212F83B9-2B24-11D7-8648000102C1865D

Jafarzadeh, M., Shoghani-Motlagh, M., Mousivand, F., Criniti, S., Critelli, S., 2022. Compositional and geochemical signatures of Oligocene volcanoclastic sandstones of Abbasabad-Kahak area, NE Iran: iImplications for provenance rela-

tions and paleogeography. Marine and Petroleum Geology, **139**: 105605; https://doi.org/10.1016/j.marpetgeo.2022.105605

Kazemi, Z., Ghasemi, H., Tilhac, R., Griffin, W., Moghadam, H.S., O'Reilly, S., Mousivand, F., 2019. Late Cretaceous subduction-related magmatism on the southern edge of Sabzevar basin, NE Iran. Journal of the Geological Society, **176**: 530–552; https://doi.org/10.1144/jgs2018-076

Malekzadeh, M., Hosseini-Barzi, M., Sadeghi, A., Critelli, S., 2020. Geochemistry of Asara Shale member of Karaj Formation, Central Alborz, Iran: Provenance, source weathering and tectonic setting. Marine and Petroleum Geology, **121**: 104584; https://doi.org/10.1016/j.marpetgeo.2020.104584

Mallah, M., Salehi, M.A., Jafarzadeh, M., Mazroei Sebdani, Z., 2022. Facies and sedimentary environment of the lower Akhoreh Fm (Middle Eocene), Shurab section, north of Nain. Applied Sedimentology, **10**: 169–185; https://doi.org/10.22084/PSJ.2021.25100.1315

Marsaglia, K.M., Barone, M., Critelli, S., Busby, C., Fackler-Adams, B., 2016. Petrography of volcaniclastic rocks in intra-arc volcano-bounded to fault-bounded basins of the Rosario segment of the Lower Cretaceous Alisitos oceanic arc, Baja California, Mexico. Sedimentary Geology, **336**: 138–146; https://doi.org/10.1016/j.sedgeo.2015.11.008

Mattei, M., Cifelli, F., Muttoni, G., Rashid, H., 2015. Post-Cimmerian (Jurassic–Cenozoic) paleogeography and vertical axis tectonic rotations of Central Iran and the Alborz Mountains. Journal of Asian Earth Sciences, **102**: 92–101; https://doi.org/10.1016/j.jseaes.2014.09.038

McLennan, S.M., Taylor, S.R., Eriksson, K.A., 1983. Geochemistry of Archean shales from the Pilbara Supergroup, Western Australia. Geochimica et Cosmochimica Acta, **47**: 1211–1222; https://doi.org/10.1016/0016-7037(83)90063-7

McLennan, S.M., Hemming, S., McDaniel, D.K., Hanson, G.N., 1993. Geochemical approaches to sedimentation, provenance and tectonics. GSA Special Paper, **284**: 21–40; https://doi.org/10.1130/SPE284-p21

Meinhold, G., Kostopoulos, D., Reischmann, T., Frei, D., BouDagher-Fadel, M.K., 2009. Geochemistry, provenance and stratigraphic age of metasedimentary rocks from the eastern Vardar suture zone, northern Greece. Palaeogeography, Palaeoclimatology, Palaeoecology, **277**: 199–225; https://doi.org/10.1016/j.palaeo.2009.04.005

Mouthereau, F., Lacombe, O., Vergés, E., 2012. Building the Zagros collisional orogen: Timing, strain distribution and the dynamics of Arabia/Eurasia plate convergence. Tectonophysics, **532–535**: 27–60; https://doi.org/10.1016/j.tecto.2012.01.022

Nesbitt, H.W., Young, G.M., 1982. Early Proterozoic climates and plate motions inferred from major element chemistry of lutites. Nature, **299**: 715–717; https://doi.org/10.1038/299715a0

Pettijohn, F.J., Potter, P.E., Siever, R., 1972. Sand and Sandstone. Springer, Berlin.

Pirnia, T., Arai, S., Torabi, G., 2013. A better picture of the mantle section of the Nain Ophiolite inferred from detrital chromian spinels. The Journal of Geology, **121**: 645–661; https://doi.org/10.1086/673175

Pirnia, T., Saccani, E., Torabi, G., Chiari, M., Goričan, Š., Barbero, E., 2020. Cretaceous tectonic evolution of the Neo-Tethys in Central Iran: evidence from petrology and age of the Nain-Ashin ophiolitic basalts. Geoscience Frontiers, **11**: 57–81; https://doi.org/10.1016/j.gsf.2019.02.008

Pourdivanbeigi Moghaddam, S., Salehi, M.A., Jafarzadeh, M., Zohdi, A., 2020. Provenance, palaeoweathering and tectonic setting of the Ediacaran Bayandor Formation in NW Iran: Implications for the northern Gondwana continental margin during the late Neoproterozoic. Journal of African Earth Sciences, **161**: 103670; https://doi.org/10.1016/j.jafrearsci.2019.103670

Purevjav, N., Roser, B., 2013. Geochemistry of Silurian–Carboniferous sedimentary rocks of the Ulaanbaatar terrane, Hangay–Hentey belt, central Mongolia: provenance, paleoweathering, tectonic setting, and relationship with the neighbouring Tsetserleg terrane. Geochemistry, **73**: 481–493; https://doi.org/10.1016/j.chemer.2013.03.003

Ramezani, J., Tucker, R.D., 2003. The Saghand Region, Central Iran: U-Pb geochronology, petrogenesis and implications for Gondwana Tectonics. American Journal of Science, **303**: 622–665; https://doi.org/10.2475/ajs.303.7.622

Ramos-Vázquez, M.A., Armstrong-Altrin, J.S., 2019. Sediment chemistry and detrital zircon record in the Bosque and Paseo del Mar coastal areas from the southwestern Gulf of Mexico. Marine and Petroleum Geology, **110**: 650–675; https://doi.org/10.1016/j.marpetgeo.2019.07.032

Ramos-Vázquez, M.A., Armstrong-Altrin, J.S., Madhavaraju, J., Gracia, A., Salas-de-León, D.A., 2022. Mineralogy and Geochemistry of Marine Sediments in the Northeastern Gulf of Mexico. In: Geochemical Treasures and Petrogenetic Processes (eds. J.S. Armstrong-Altrin, K. Pandarinath and S. Kumar Verma): 153–183. Springer; https://doi.org/10.1007/978-981-19-4782-7_7

Roser, B.P., Korsch, R.J., 1986. Determination of tectonic setting of sandstone-mudstone suites using SiO_2 content and K_2O/Na_2O ratio. Geology, **94**: 635–650; https://doi.org/10.1086/629071

Rudnick, R.L., Gao, S., 2003. Composition of the Continental Crust. Elsevier; https://doi.org/10.1016/B0-08-043751-6/03016-4

Salehi, M.A., Moussavi-Harami, S.R., Mahboubi, A., Wilmsen, M., Heubeck, C., 2014. Tectonic and paleogeographic implications of compositional variations within the siliciclastic Ab-Haji Formation (Lower Jurassic, east Central Iran). Neues Jahrbuch für Geologie und Paläontologie Abhandlungen, **271**: 21–48; https://doi.org/10.1127/0077-7749/2014/0373

Shafaii Moghadam, H., Whitechurch, H., Rahgoshay, M., Monsef, I., 2009. Significance of Nain-Baft ophiolitic belt (Iran): short-lived, transtensional Cretaceous back-arc oceanic basins over the Tethyan subduction zone. Comptes Rendus Geosciences, **341**: 1016–1028; https://doi.org/10.1016/j.crte.2009.06.011

Shirdashtzadeh, N., Torabi, G., 2020. Serpentinization and chloritization of metamorphosed lherzolites in Darreh-Deh (east of Nain Ophiolite, Central Iran): calcium source for rodingitization and tremolitization. Neues Jahrbuch für Mineralogie Abhandlungen, **196**: 179–191; https://doi.org/10.1127/njma/2019/0163

Shirdashtzadeh, N., Torabi, G., Meisel, T., Arai, S., Bokhari, S.N.H., Samadi, R., Gazel, E., 2014. Origin and evolution of metamorphosed mantle peridotites of Darreh Deh (Nain Ophiolite, Central Iran): Implications for the Eastern Neo-Tethys evolution. Neues Jahrbuch für Geologie und Paläontologie Abhandlungen, **273**: 89–120; https://doi.org/10.1127/0077-7749/2014/0418

Shirdashtzadeh, N., Kachovich, S., Aitchison, J.C., Samadi, R., 2015. Mid-Cretaceous radiolarian faunas from the Ashin Ophiolite (western Central-East Iranian Microcontinent). Cretaceous Research, **56**: 110–118; https://doi.org/10.1016/j.cretres.2015.04.003

Suttner, L.J., Dutta, P.K., 1986. Alluvial sandstone composition and paleoclimate; I, Framework mineralogy. Journal of Sedimentary Petrology, **56**: 329–345; https://doi.org/10.1306/212F8909-2B24-11D7-8648000102C1865D

Tadayon, M., Rossetti, F., Zattin, M., Nozaem, R., Calzolari, G., Madanipour, S., Salvini, F., 2017. The Post-Eocene evolution of the Doruneh Fault Region (Central Iran): the intraplate response to the reorganization of the Arabia-Eurasia Collision Zone. Tectonics, **36**: 3038–3064; https://doi.org/10.1002/2017TC004595

Tadayon, M., Rossetti, F., Zattin, M., Calzolari, G., Nozaem, R., Salvini, F., Faccenna, C., Khodabakhshi, P., 2019. The long-term evolution of the Doruneh Fault region (Central Iran): a key to understanding the spatio-temporal tectonic evolution in the hinterland of the Zagros convergence zone. Geological Journal, **54**: 1454–1479; https://doi.org/10.1002/gj.3241

Taheri, A., Jafarzadeh, M., Armstrong-Altrin, J., Mirbagheri, S.R., 2018. Geochemistry of siliciclastic rocks from the Shemshak Group (Upper Triassic–Middle Jurassic), northeast-

ern Alborz, northern Iran: implications for palaeoweathering, provenance, and tectonic setting. Geological Quarterly, **62** (3): 522–535; https://doi.org/10.7306/gq.1433

Torabi, G., Shirdashtzadeh, N., Arai, S., Koepke, J., 2011. Paleozoic and Mesozoic ophiolites of Central Iran: amphibolites from Jandaq, Posht-e-Badam, Nain and Ashin ophiolites. Neues Jahrbuch für Geologie und Paläontologie Abhandlungen, **262**: 227–240; https://doi.org/10.1127/0077-7749/2011/0194

Ulmer-Scholle, D.S., Scholle, P.A., Schieber, J., Raine, R.J., 2015. A color guide to the petrography of sandstones, siltstones, shales and associated rocks. AAPG Memoir, **109**; https://doi.org/10.1306/M1091304

Verdel, C., Wernicke, B.P., Hassanzadeh, J., Guest, B., 2011. A Paleogene extensional arc flare-up in Iran. Tectonics, **30**: TC3008; https://doi.org/10.1029/2010TC002809

Verma, S.P., Armstrong-Altrin, J.S., 2013. New multi-dimensional diagrams for tectonic discrimination of siliciclastic sediments and their application to Precambrian basins. Chemical Geology, **355**: 117–133; https://doi.org/10.1016/j.chemgeo.2013.07.014

Wilmsen, M., Fursich, F.T., Seyed-Emami, K., Majidifard, M.R., 2009. An overview of the stratigraphy and facies development of the Jurassic System on the Tabas Block, east-central Iran. Geological Society Special Publications, **312**: 323–343; https://doi.org/10.1144/SP312.15

Zaid, S.M., 2015. Geochemistry of sandstones from the Pliocene Gabir Formation, north Marsa Alam, Red Sea, Egypt: implication for provenance, weathering and tectonic setting. Journal of African Earth Sciences, **102**: 1–17; https://doi.org/10.1016/j.jafrearsci.2014.10.016